

Article

Modeling and Assessing Potential Soil Erosion Hazards Using USLE and Wind Erosion Models in Integration with GIS Techniques: Dakhla Oasis, Egypt

Salman A. H. Selmy ^{1,*} , Salah H. Abd Al-Aziz ¹, Raimundo Jiménez-Ballesta ² , Francisco Jesús García-Navarro ³  and Mohamed E. Fadl ⁴ 

¹ Department of Soils and Water, Faculty of Agriculture, Assiut University, Assiut 71526, Egypt; salah.abdelaziz@agr.aun.edu.eg

² Department of Geology and Geochemistry, Autonomous University of Madrid, 28019 Madrid, Spain; raimundo.jimenez@uam.es

³ High Technical School of Agricultural Engineers, University of Castilla-La Mancha, 13007 Ciudad Real, Spain; fcojesus.garcia@uclm.es

⁴ Division of Scientific Training and Continuous Studies, National Authority for Remote Sensing and Space Sciences (NARSS), Cairo 11769, Egypt; madham@narss.sci.eg

* Correspondence: salman.selmy@agr.aun.edu.eg; Tel.: +20-111-440-9714



Citation: Selmy, S.A.H.; Abd Al-Aziz, S.H.; Jiménez-Ballesta, R.; García-Navarro, F.J.; Fadl, M.E. Modeling and Assessing Potential Soil Erosion Hazards Using USLE and Wind Erosion Models in Integration with GIS Techniques: Dakhla Oasis, Egypt. *Agriculture* **2021**, *11*, 1124. <https://doi.org/10.3390/agriculture11111124>

Academic Editor: Carlos Asensio Grima

Received: 16 October 2021

Accepted: 8 November 2021

Published: 10 November 2021

Publisher's Note: MDPI stays neutral with regard to jurisdictional claims in published maps and institutional affiliations.



Copyright: © 2021 by the authors. Licensee MDPI, Basel, Switzerland. This article is an open access article distributed under the terms and conditions of the Creative Commons Attribution (CC BY) license (<https://creativecommons.org/licenses/by/4.0/>).

Abstract: Soil erosion modeling is becoming more significant in the development and implementation of soil management and conservation policies. For a better understanding of the geographical distribution of soil erosion, spatial-based models of soil erosion are required. The current study proposed a spatial-based model that integrated geographic information systems (GIS) techniques with both the universal soil loss equation (USLE) model and the Index of Land Susceptibility to Wind Erosion (ILSWE). The proposed Spatial Soil Loss Model (SSLM) was designed to generate the potential soil erosion maps based on water erosion and wind erosion by integrating factors of the USLE and ILSWE models into the GIS environment. Hence, the main objective of this study is to predict, quantify, and assess the soil erosion hazards using the SSLM in the Dakhla Oasis as a case study. The water soil loss values were computed by overlaying the values of five factors: the rainfall factor (R-Factor), soil erodibility (K-Factor), topography (LS-Factor), crop types (C-Factor), and conservation practice (P-Factor). The severity of wind-driven soil loss was calculated by overlaying the values of five factors: climatic erosivity (CE-Factor), soil erodibility (E-Factor), soil crust (SC-Factor), vegetation cover (VC-Factor), and surface roughness (SR-Factor). The proposed model was statistically validated by comparing its outputs to the results of USLE and ILSWE models. Soil loss values based on USLE and SSLM varied from 0.26 to 3.51 t ha⁻¹ yr⁻¹ with an average of 1.30 t ha⁻¹ yr⁻¹ and from 0.26 to 3.09 t ha⁻¹ yr⁻¹ with a mean of 1.33 t ha⁻¹ yr⁻¹, respectively. As a result, and according to the assessment of both the USLE and the SSLM, one soil erosion class, the very low class (<6.7 t ha⁻¹ yr⁻¹), has been reported to be the prevalent erosion class in the study area. These findings indicate that the Dakhla Oasis is slightly eroded and more tolerable against water erosion factors under current management conditions. Furthermore, the study area was classified into four classes of wind erosion severity: very slight, slight, moderate, and high, representing 1.0%, 25.2%, 41.5%, and 32.3% of the total study area, respectively, based on the ILSWE model and 0.9%, 25.4%, 43.9%, and 29.9%, respectively, according to the SSLM. Consequently, the Dakhla Oasis is qualified as a promising area for sustainable agriculture when appropriate management is applied. The USLE and ILSWE model rates had a strong positive correlation ($r = 0.97$ and 0.98 , respectively), with the SSLM rates, as well as a strong relationship based on the average linear regression ($R^2 = 0.94$ and 0.97 , respectively). The present study is an attempt to adopt a spatial-based model to compute and map the potential soil erosion. It also pointed out that designing soil erosion spatial models using available data sources and the integration of USLE and ILSWE with GIS techniques is a viable option for calculating soil loss rates. Therefore, the proposed soil erosion spatial model is fit for calculating and assessing soil loss rates under this study and is valid for use in other studies under arid regions with the same conditions.

Keywords: soil erosion hazard; USLE; ILSWE; GIS techniques; soil erosion spatial modeling; soil erosion mapping; soil conservation; erosion factors

1. Introduction

Soil erosion is the most significant factor in land degradation because it causes soil particles to be transported and deposited from one site to another by wind or water [1,2]. This type of soil degradation deteriorates soil quality, such as, among others, soil compaction, reducing soil organic matter, drainage problems, loss of soil structure, declining crop yields, loss of soil nutrients, and soil productivity reduction [3,4]. Soil erosion is one of the most serious forms of soil degradation, particularly on agricultural land, as it threatens both agronomic productivity and environmental quality [5], and the erosion caused by water can be severe, especially when the soil is bare [6]. Furthermore, a large proportion of total soil erosion over a long time is generally due to a few heavy storms [7].

Human activities, and biogeochemical, biophysical, and hydrological factors, frequently aggravate soil erosion. Soil erosion rates and soil erosion susceptibility maps provide information on vulnerable areas. However, soil erosion assessment processes are very complex given their multifactorial influences [8–10], which may explain why there are several mathematical models for estimating soil erosion. Karydas et al. [11] identified 82 soil erosion models and classified them into eight geospatial categories. Of the numerous erosion models, three types of soil erosion models exist based on the nature of basic algorithms, which are (i) physics-based, (ii) empirical, and (iii) conceptual models [12]. Empirical-based models have been particularly widespread in soil erosion assessments. The universal soil loss equation (USLE), developed by Wischmeier and Smith [13], has been widely used to predict long-term soil loss caused by water erosion. This model has been applied to semiarid zones but less frequently to arid regions [14–19]. Attempts to improve empirical soil loss equations are still ongoing [20] as these approaches are still appealing from a practical point of view [21].

The USLE model had some spatial distribution limitations at first, which were overcome by combining geospatial techniques [22]. Geoinformatics technologies, such as geographic information systems (GIS) and remote sensing, help to acquire various types of data. These data are then integrated with various soil erosion models to assess soil erosion [23,24]. Many studies have been carried out using various soil erosion models combined with geoinformatics techniques [23–27]. Thus, geoinformatics techniques, as a very accurate method, play a vital role in data collection, analyses, and validation by providing information on soil erosion dynamics and intensity [22,27–31]. According to the USLE, several kinds of data and information are required, such as climate data, topographical elements, soil characteristics, land use, and land cover. In the ArcGIS environment of the model builder, these data were rated and weighed for quantifying and performing soil erosion in the spatially distributed methodologies used for this study.

Fenta et al. [32] developed a wind erosion index by integrating five relevant factors using a fuzzy logic technique and compared it with estimates of the frequency of dust storms derived from long-term Sea-Viewing Wide Field-of-View Sensor Level-3 daily data. This index provides new insights into the spatial patterns of wind erosion risks in East Africa and can be used to prioritize areas.

Major civil, industrial, and agricultural activities have been planned in the Western Desert, which covers 66.7% of the total area of Egypt, and includes some depressions, i.e., Kharga, Farafra, Dakhla, Bahariya, Qattara, Siwa, and El Fayum. The Nubian Sandstone Aquifer (NSSA), located in this desert, is the largest groundwater aquifer in Egypt [33]. An oasis is an area made fertile by a source of fresh water in an arid region (desert). Oases (more than one oasis) are irrigated by natural springs or other underground water sources. Oases also provide habitats for animals and plants. Oases can be found in the desert regions of the Arabian Peninsula, Egypt's Sahara Desert, and many other desert regions around

the world, including Peru, Tunisia, Niger, and others. The Dakhla Oasis has agricultural expansion potential due to high groundwater quantities and soil fertility, and it is the main oasis that supports a large human population [34]. Land degradation is a common serious issue in agricultural production, and many methodologies are available for appreciating soil development extensions. The quantification and statistical analysis of soil degradation assessments depend on a variety of soil characteristics. It requires different data forms and information on soil properties [35].

Quantitative and spatial assessments of environmental hazards are needed because the soil erosion, salinity, and sodicity risks have become serious problems in some areas of Egypt, where soil quality degradation has increased. With wide spatial diversity and data limitations, the USLE equation is used for predicting and calculating soil loss. The GIS database and analysis are critical for observing and assessing soil environmental hazards in the study area [36]. In the geographic information systems (GIS) modeling environment, the proposed spatial model was designed and developed for soil erosion assessment based on the USLE factors' rates and land characteristics. Therefore, by overlaying thematic layers, ratings, and weighing soil parameters' data, action can be taken to achieve more effective land use planning and management [37,38]. GIS is a modern technique for processing, displaying, analyzing, and storing large amounts of spatial data in a variety of formats and scales. Therefore, it provides accessible assessment, quantification, and performance of soil information. A GIS analysis provides continuous spatial datasets, including spatially referenced modeling, and covers large areas [39]. In Egypt's desert oases, soil erosion is a severe environmental hazard, with some areas vulnerable to catastrophic erosion loss if favorable conditions exist. This is due to its arid climate, scarce vegetation cover, bare lands, soil types, topographic features, and lack of soil and water conservation practices. The proposed model can be validated by comparing its outcomes to those of the recommended validated models. In the current study, this was accomplished by comparing soil erosion rates calculated using USLE and wind erosion models (validation-models) to rates calculated using the proposed model. So, the main objective of the present work was to assess the performance of a proposed spatial-based model designed based on USLE and wind erosion models in predicting, quantifying, and assessing the soil erosion hazards in Dakhla Oasis, Egypt.

2. Materials and Methods

2.1. Study Area Description

The Dakhla Oasis is one of seven oases in Egypt's Western Desert. It extends 80 km from east to west and 25 km from north to south and is located between 28°14'00" and 30°00'00" E and 25°09'00" and 25°58'00" N (Figure 1). The study area of the Dakhla Oasis is made up of several communities connected by a string of sub oases, and it covers 4952.15 km² (495,215 ha). Sediments from the Upper Cretaceous to the Lower Eocene and Quaternary eras cover the study area [40].

The Dakhla Oasis has a hot desert climate, where "Hyperthermic" is the soil temperature regime, and "Torric" is the moisture regime [41]. The National Oceanic and Atmospheric Administration (NOAA) [42] was the source of climate data for the study area, as shown in Table 1. The floor of the Dakhla depression as a physiographic unit represents arable lands for agriculture and orchards in the study area. According to Soil Taxonomy (2014), the dominant soil orders in the study area are Aridisols, Inceptisols, and Entisols [43,44].

Advanced remote sensing techniques and DEM interpretation methods were used to identify physiographic units using digital satellite images and field studies that provide the ground observation reality. The study area was categorized into eight physiographic units: (1) depression, (2) Palaya basins, (3) mesas, (4) residual hills, (5) rocky lands, (6) sand dunes, (7) sand sheets, and (8) waterbodies. These physiographic units are illustrated in Figure 2 and their characteristics are shown in Table 2.

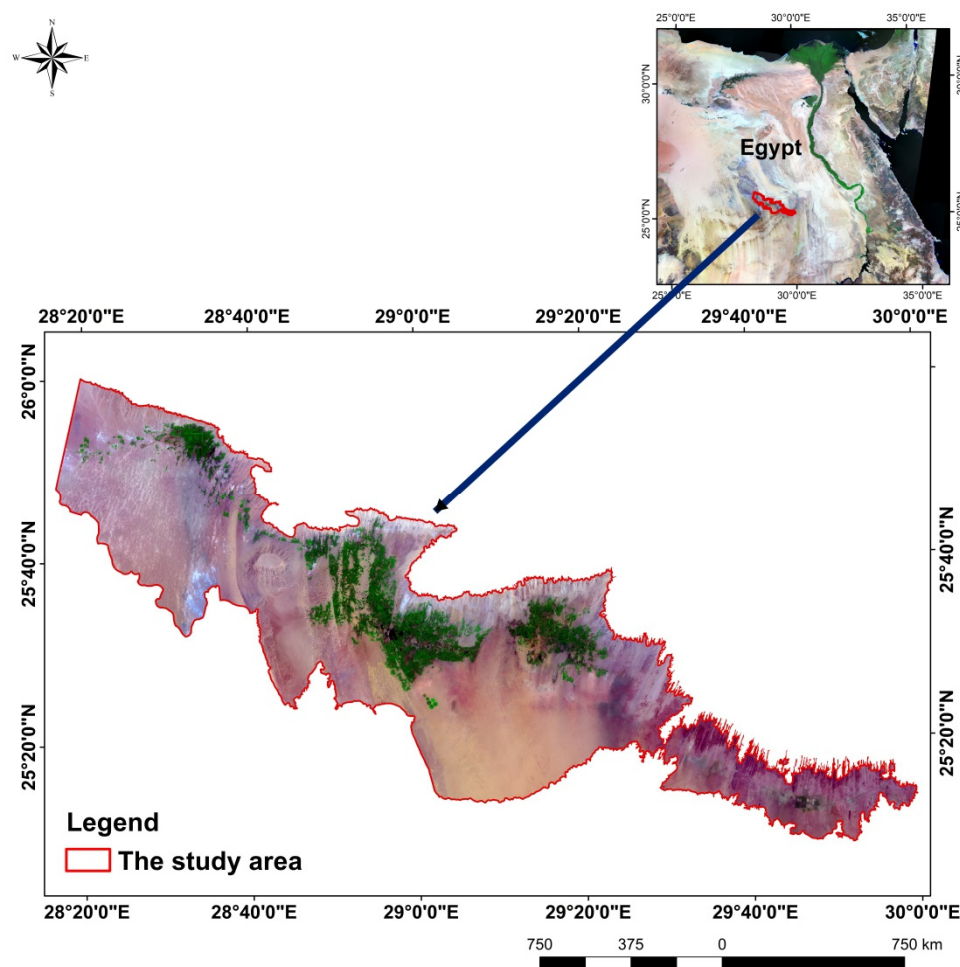


Figure 1. Location map of the study area relative to Egypt map.

Table 1. Climatic data for Dakhla Oasis.

Month	Jan	Feb	Mar	Apr	May	Jun	Jul	Aug	Sep	Oct	Nov	Dec	Year
High tem. °C	33	40	45	46	48	50	45	46	45	44	39	33	49.5
Daily mean tem. °C	12	14	18	24	28	31	31	30	28	24	18	14	22.8
Low tem. °C	3.5	5.1	8.7	13	18	22	22	22	20	16	9.9	5.3	13.8
Precipitation average (mm)	1.0	0.1	0.1	0.99	0.99	0.1	0.1	0.99	0.99	0.1	0.1	0.1	0.1
Relative humidity (%)	47	41	35	29	26	24	26	28	31	36	43	47	34.4
Evapotranspiration (mm)	3.3	4.1	5.4	6.9	8.6	8.8	8.9	8.2	7.1	5.6	3.9	2.9	6.1
Wind velocity (ms ^{−1})	2.5	2.5	2.7	3.1	3.6	3.3	3.1	3.1	3.1	3.1	2.5	2.5	2.9

tem. = temperature.

Table 2. The physiographic units of the study area.

No.	Physiographic Unit	Code	Area (km ²)	Area (%)
1	Depression	D	1921.65	38.8
2	Palaya plains	BP	181.12	3.7
3	Sand dunes	SD	268.14	5.4
4	Sand sheets	SSH	343.74	6.9
5	Barren land	RL	2104.48	42.5
6	Mesa	M	61.13	1.2
7	Residual hills	RH	45.32	0.9
8	Waterbodies	L	26.57	0.5
Total			4952.15	100.0

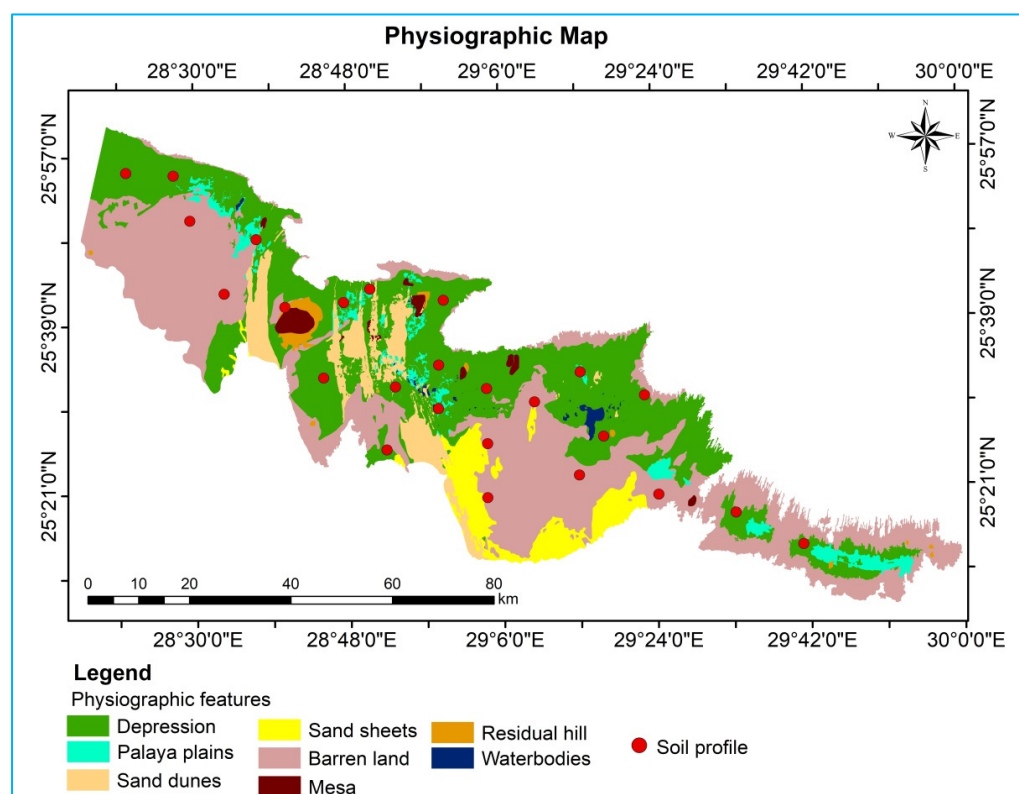


Figure 2. The physiographic map of the study area and sampling sites.

2.2. Digital Images Processing

Geometrically, the Landsat-8 image (Path 177, Row 42, and year 2020) of the investigated area and Shuttle Radar Topography Mission (SRTM) data were used to produce the digital elevation model (DEM, 90 m resolution) of the studied area. The image was draped over the DEM using the ENVI 5.1 software to identify and delineate the map of physiographic units [45]. The study area maps of physiographic features, soil erosion factors, and soil loss rates were created using ArcGIS 10.2.2 software [46].

2.3. Field Survey and Laboratory Analyses

Twenty-five geo-referenced soil profiles using the Global Position System (GPS) were chosen based on a physiographical map (Figure 2). Soil profiles were dug and described according to the Soil Science Division Staff [47]. Following the standard Soil Survey Staff methods [48], soil samples were analyzed in the laboratory for particle size distribution (sand, silt, and clay), using the pipette method, soil organic matter content (OM) by Walkley–Black method, and calcium carbonate content employing the Calcimeter Scheibler’s method.

2.4. The Universal Soil Loss Equation (USLE) Model

Wischmeier and Smith [13] proposed the USLE, which has been widely used, and still is used in many areas of the world. The USLE is an empirical-based model designed to predict, quantify, and assess the annual average soil loss rate for a given area under particular management conditions. This equation is calculated based on certain study area factors, such as slope, rainfall erosivity, soil type, topography elements, crop system, and management practices. These factors are a numerical representation of the particular conditions that influence the soil erosion risk in the region under study [13]. According to Robert and Hilborn [49], soil erosion values and rates reveal that soil factors can largely be

attributed to variations in management conditions, as shown in Tables 3 and 4 and Figure 3. The soil loss rate is expressed in the USLE model as follows:

$$A = R \times K \times LS \times C \times P \quad (1)$$

where A is the predicted annual mean soil loss ($\text{t ha}^{-1} \text{yr}^{-1}$), R is the rainfall erosivity factor ($\text{MJ mm ha}^{-1} \text{h}^{-1} \text{yr}^{-1}$), K is the soil erodibility factor ($\text{t ha h ha}^{-1} \text{MJ}^{-1} \text{mm}^{-1}$), LS is the topographic factor (dimensionless), C is the land cover and management factor (crop types and tillage) (dimensionless), and P is the conservation practice factor (dimensionless).

Table 3. Management strategies for reducing soil erosion.

Factor	Management Strategies	Example
R	The R factor for a field cannot be change.	-
K	The K factor for a field cannot be change.	-
LS	Terraces may be constructed to reduce the slope length resulting in lower soil losses.	Terracing requires additional investment and will cause some inconvenience in farming. Investigate other soil conservation practices first.
C	Crop types and tillage methods that result in the lowest possible C factor will result in less soil erosion.	Cropping systems that will provide maximum protection for the soil. Use minimum tillage systems where possible.
P	Support practice that has the lowest possible factor associated with it will result in lower soil losses.	Use support practices such as cross-slope farming that will cause deposition of sediment to occur close to the source.

R = rainfall erosivity factor; K = soil erodibility factor; LS = topographic factor; C = land cover and management factor; P = conservation practice factor.

Table 4. Soil erosion classes and the corresponding soil loss rates.

Soil Erosion Class	Soil Loss Rate ($\text{t ha}^{-1} \text{yr}^{-1}$)
Very low (tolerable)	<6.7
Low	6.7–11.2
Moderate	11.2–22.4
High	22.4–33.6
Severe	>33.6

2.4.1. Rainfall Erosivity (R -Factor)

The R -Factor quantifies soil erosivity based on the aggressiveness of runoff sediment deposits in a specific area over a given time period. Therefore, the rainfall erosivity factor represents the amount and rate of runoff caused by precipitation events [50]. Based on the annual maximum precipitation in 24 h during the study period, the R -Factor was calculated using the empirical Equation (2) developed by Chaudhry and Nayak [51].

$$R_a = 79 + (0.363 * X_a) + 89.7 \quad (2)$$

where R_a is the rainfall erosivity factor ($\text{MJ mm ha}^{-1} \text{h}^{-1} \text{yr}^{-1}$) and X_a is the annual precipitation average (mm).

The R -Factor was estimated using the climatological data from the NOAA [42]. The R -Factor map was digitized and interpolated using the point-to-raster interpolation tool in the ArcGIS software (geostatistic analysis).

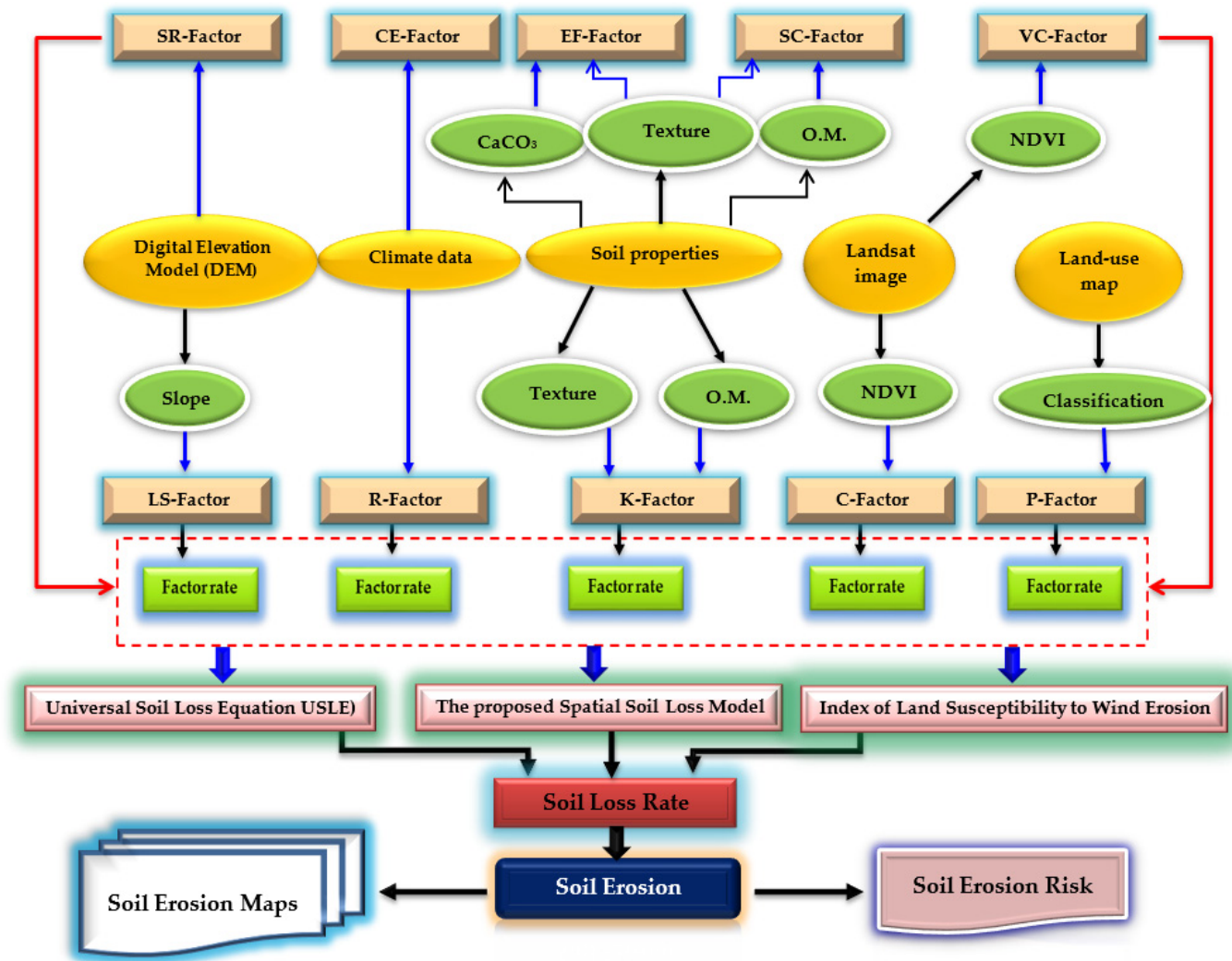


Figure 3. A flowchart of soil erosion quantification.

2.4.2. Soil Erodibility (K-Factor)

One of the most significant barriers for soil erosion modeling on large spatial scales is the insufficient data on soil attributes [52,53]. The K-Factor describes the predisposition of soil particles to be transported and separated by runoff. The K-Factor is rated primarily on a scale of 0 to 1, where 0 is low predisposition for soil erosion and 1 is highly predisposed. The K-Factor rate values depend on soil texture classes, soil structure stability, soil mineralogy, organic matter content, soil permeability, and infiltration. Wischmeier et al. [54] developed an equation to rate K-Factor using the empirical equation, and the K-Factor values for different soil textures were estimated using Equation (3).

$$100K = 2.1M^{1.14}(10)^{-4}(12 - a) + 3.25(b - 2) + 2.5(c - 3) \quad (3)$$

where K is the soil erodibility factor, M is the soil particle size distribution parameter calculated as [very fine sand (%) + silt (%)] \times [100 – Clay (%)], a is the soil organic matter (%), b is the soil structure code, and c is the soil profile permeability class.

Robert and Hilborn [49] clarified the K-Factor rates for various soil textures, as shown in Table 5.

Table 5. Different soil types and the corresponding rates of soil erodibility factor (K-Factor).

Soil Texture	K-Factor Rate			Soil Texture	K-Factor Rate		
	O.M. Mean	O.M. < 2%	O.M. > 2%		O.M. Mean	O.M. < 2%	O.M. > 2%
Clay	0.49	0.54	0.47	Loamy very fine sand	0.87	0.99	0.56
Clay loam	0.67	0.74	0.63	Sand	0.04	0.07	0.02
Coarse sandy loam	0.16	–	0.16	Sandy clay loam	0.45	–	0.45
Fine sand	0.18	0.20	0.13	Sandy loam	0.29	0.31	0.27
Fine sandy loam	0.40	0.49	0.38	Silt loam	0.85	0.92	0.83
Heavy clay	0.38	0.43	0.34	Silty clay	0.58	0.61	0.58
Loam	0.67	0.76	0.58	Silty clay loam	0.72	0.79	0.67
Loamy fine sand	0.25	0.34	0.20	Very fine sand	0.96	1.03	0.83
Loamy sand	0.09	0.11	0.09	Very fine sandy loam	0.79	0.92	0.74

O.M. = organic matter.

2.4.3. Slope Length and Slope Gradient (LS-Factor)

The *LS*-Factor is expressed as the ratio extracted from the DEM image and the computation using GIS-based methods. The *LS*-Factor was used in the USLE to assess the local topography effect on soil erosion per unit zone. Based on topographic effects on soil erosion and cutting rates, the runoff on longer slopes with the greatest accumulation increases its transport detachment and capacity. The *LS*-Factor can be used to express the soil erosion ratio as defined by Wischmeier and Smith [13] and expressed as Equation (4).

$$LS = (L/22.1)^m (0.065 + 0.045 S + 0.0065 S)^2 \quad (4)$$

where *L* is the slope length (m) and *S* is the slope gradient (%).

The *LS*-Factor rates for topography effects were explained by Robert and Hilborn [49] and are shown in Table 6.

Table 6. Slope length and slope steepness factors (*LS*-Factor) data.

	Slope (%)	L.S-F	Slope (%)	L.S-F	Slope (%)	L.S-F	Slope (%)	L.S-F	Slope (%)	L.S-F	Slope (%)	L.S-F
Slope Length (m)	30.5		61		122		244		488		975	
10	1.38		10	1.95	10	2.76	10	3.90	10	5.52	10	7.81
8	1.00		8	1.41	8	1.99	8	2.82	8	3.99	8	5.64
6	0.67		6	0.95	6	1.35	6	1.91	6	2.70	6	3.81
5	0.54		5	0.76	5	1.07	5	1.52	5	2.15	5	3.03
4	0.40		4	0.53	4	0.70	4	0.92	4	1.21	4	1.60
3	0.30		3	0.39	3	0.52	3	0.68	3	0.90	3	1.19
2	0.20		2	0.25	2	0.30	2	0.37	2	0.46	2	0.57
1	0.13		1	0.16	1	0.20	1	0.24	1	0.30	1	0.36
0	0.07		0	0.08	0	0.09	0	0.11	0	0.12	0	0.14

L.S-F = *LS*-Factor.

2.4.4. Cropping Management (C-Factor)

The *C*-Factor is used to determine and reflect the impacts of both land cover and land management, on various vegetation types. The vegetation cover factor and the *LS*-Factor are very sensitive to potential tilled soil erosion values under defined conditions and, thus, differ depending on the adopted soil conservation practices. In this study, the *C*-Factor was assessed using the Normalized Difference Vegetation Index (NDVI), which is expressed by Equation (5) [55].

$$C = \exp\left[\alpha \frac{NDVI}{(\beta - NDVI)}\right] \quad (5)$$

where *C* is crop management (*C*-Factor), and α and β are the parameters that determine the shape of the curve relating to NDVI.

The *C*-Factor rates for crop management were explained by Robert and Hilborn [49] and are shown in Tables 7 and 8.

Table 7. Crop type factor (C1-Factor) scores.

Crop Type	C1-Factor	Crop Type	C1-Factor
Grain corn	0.40	Agriculture	0.6
Silage corn, beans, and canola	0.50	Forest	0.13
Cereals (spring and winter)	0.35	Waste land	0.85
Seasonal horticultural crops	0.55	Orchids	0.42
Fruit trees	0.10	Bare lands	1
Hay and pasture	0.02	-	-

Table 8. Tillage method factor (C2-Factor) scores.

Tillage Method	C2-Factor	Tillage Method	C2-Factor	Tillage Method	Factor
Fall plow	1.0	Mulch tillage	0.60	Zone tillage	0.25
Spring plow	0.90	Ridge tillage	0.35	No-till	0.25

2.4.5. Conservation Practice (P-Factor)

The P-Factor is a support practice factor that represents the soil loss ratio of up- and down slope tillage. It acts through altering the flow pattern, gradients, or direction of surface runoff with specific support and expressed land practice effects that reduce the amount of runoff and erosion [14]. The P-Factor is an important consideration in the USLE equation model for mapping conservation practices using classified images of land use/land cover and slope. These images include different types of agricultural management support practices, such as up-and-down sloping, cross sloping, strip cropping, contour farming, and terracing. The P-Factor rates for conservation support practices, as represented by Robert and Hilborn [49], are shown in Table 9.

Table 9. Conservation practice (P-Factor) data.

Support Practice	P-Factor	Support Practice	P-Factor	Support Practice	P-Factor
Up-and-down slope	1.0	Contour farming	0.50	Strip cropping, contour	0.25
Cross slope	0.75	Strip cropping, cross slope	0.37	-	-

2.5. Index of Land Susceptibility to Wind Erosion (ILSWE) Model

Wind erosion is a complex process with numerous factors and indicators, making it difficult to define comprehensive criteria for assessing factors at regional scales. As a result, studies of wind erosion at the regional scale employ a complexity reduction strategy while retaining the main wind erosion factors [56]. Therefore, Fenta et al. [32] developed the Index of Land Susceptibility to Wind Erosion (ILSWE), which was used in this study to estimate and assess soil erosion severity and risks by combining layers describing the major factors: climatic erosivity, soil erodibility, soil crust, vegetation cover, and surface roughness. The ILSWE index outcomes were classified into five classes using the variance minimization classification scheme: very slight (0–2), slight (2–10), moderate (10–20), high (20–50), and very high (>50) erosion severity. The general methodological framework used to assess ILSWE is described in Equation (6).

$$\text{ILSWE} = f(\text{CE} \times \text{EF} \times \text{SC} \times \text{VC} \times \text{SR}) \quad (6)$$

where CE is the climatic erosivity factor, EF is the wind-erodible fraction factor; SC is the soil crust factor, VC is the vegetation cover factor, and SR is the surface roughness factor.

2.5.1. Climatic Erosivity (CE-Factor)

Climatic erosivity (CE-Factor) is calculated according to climatic data on output conditions that are instrumental in wind erosion estimating [57]. The CE-Factor was calculated based on FAO [58] and developed in Equation (7) as follows:

$$CE = \frac{1}{100} \sum_{i=1}^{i=12} W_i^3 \left[\frac{PET_i - P_i}{PET_i} \right] \times d_i \quad (7)$$

where W_i is the mean monthly wind speed (ms^{-1}) at 2 m height in month i , PET_i is the potential evapotranspiration (mm) in month i , P_i is the precipitation (mm) in month i , and d_i is total number of days in month i .

2.5.2. Wind-Erodible Fraction (EF-Factor)

The wind erodible fraction (EF-Factor) describes the relationship between wind erosion and soil properties. The EF-Factor was calculated using the multiple regression equation (Equation (8)) proposed by Fryrear et al. [59] based on some soil properties.

$$EF = \frac{29.09 + 0.31SA + 0.17SI + 0.33\frac{SA}{CL} - 2.59SOM - 0.95CaCO_3}{100} \quad (8)$$

where EF is the wind erodible fraction factor, SA is the sand content, SI is the silt content, CL is the clay content, OM is the organic matter content, and $CaCO_3$ is the calcium carbonate content.

2.5.3. Soil Crust (SC-Factor)

In arid and semi-arid regions, wind erosion often dominates water erosion. Therefore, soil crust plays a vital role in maintaining soil resources [60]. The SC-Factor was calculated to estimate wind erosion susceptibility based on soil crust influence, which was regressed based on the clay and organic matter content coefficient of friction [61], and is determined as the following Equation (9):

$$SC = \frac{1}{1 + 0.0066(CL)^2 + 0.21(OM)^2} \quad (9)$$

2.5.4. Vegetation Cover Factor (VC-Factor)

The fractional vegetation cover that affects wind erosion by dissipating wind erosivity and providing an efficient shelter effect is defined as the VC-Factor. It was calculated using Equation (10) based on NDVI values of highly dense vegetation ($NDVI_v$) and bare soil ($NDVI_s$) derived from 2020 Landsat-8 images.

$$VC = \frac{NDVI - NDVI_s}{NDVI_v - NDVI_s} \quad (10)$$

2.5.5. Surface Roughness Factor (SR-Factor)

The SR-Factor was calculated based on the ridge height to ridge spacing ratio according to the digital elevation model (DEM) maximum, minimum, and mean using the focal statistics tools within ArcGIS 10.2.2 software as the following equation:

$$SR = \frac{DEM_{Mean} - DEM_{Min}}{DEM_{Max} - DEM_{min}} \quad (11)$$

2.6. Spatial Soil Loss Model (SSIM) Designing

According to Panagos et al. [52] and Efthimiou [53], a lack of sufficient data on soil characteristics is one of the greatest obstacles for soil erosion modeling on larger spatial scales. The integration of the USLE and the GIS techniques is globally popular for soil

erosion prediction and assessment purposes [24–26]. In the ArcGIS environment software, the proposed SSLM was designed and implemented [46]. The SSLM was performed by matching tables mathematically with the modeling environment using relational database fields through the multiplication of input rasters. The computed rates of the USLE factors (R , K , LS , C , and P) were spatially distributed using geostatistical analysis techniques (Kriging models). Then, the surface maps of soil erosion factors in a spatial zone were extracted with a unique value parameter [44]. Modeling the land susceptibility to wind erosion implied five steps: (1) selecting the criteria, (2) assigning a rating for each criterion, (3) calculating a weight for each criterion, (4) developing five factors (CE , EF , SC , VC , and SR), and (5) generating the final land susceptibility to wind erosion severity (ILSWE) map using ArcGIS software.

In this model, the final potential soil erosion spatial distribution rates and class overlay maps were created using relational database fields and the mathematical multiplication of input rasters. The thematic maps of the five factors of USLE model (R , K , LS , C , and P) and the five factors of ILSWE model (CE , EF , SC , VC , and SR) were then used to integrate them into a single soil loss rate. The soil erosion map was created by reclassifying the factor rates of the USLE and ILSWE in the GIS environment following interpolation techniques. Spatial analysis processes and overlay processes based on subclass weightage values were performed with the different thematic maps. The final maps resulted from the raster-processed weighted overlay values that provided the value of each subclass. The concept flowcharts of the SSLM for USLE and ILSWE models are shown in Figures 4 and 5, respectively.

2.7. Model Validation

Using the average linear regression method, the results of the SSLM and ILSWE were compared to the USLE model results [62]. The correlation coefficient was computed to validate the relationship between the SSLM, ILSWE, and the USLE values. SPSS package software version 22.0 was employed for the statistical analysis.

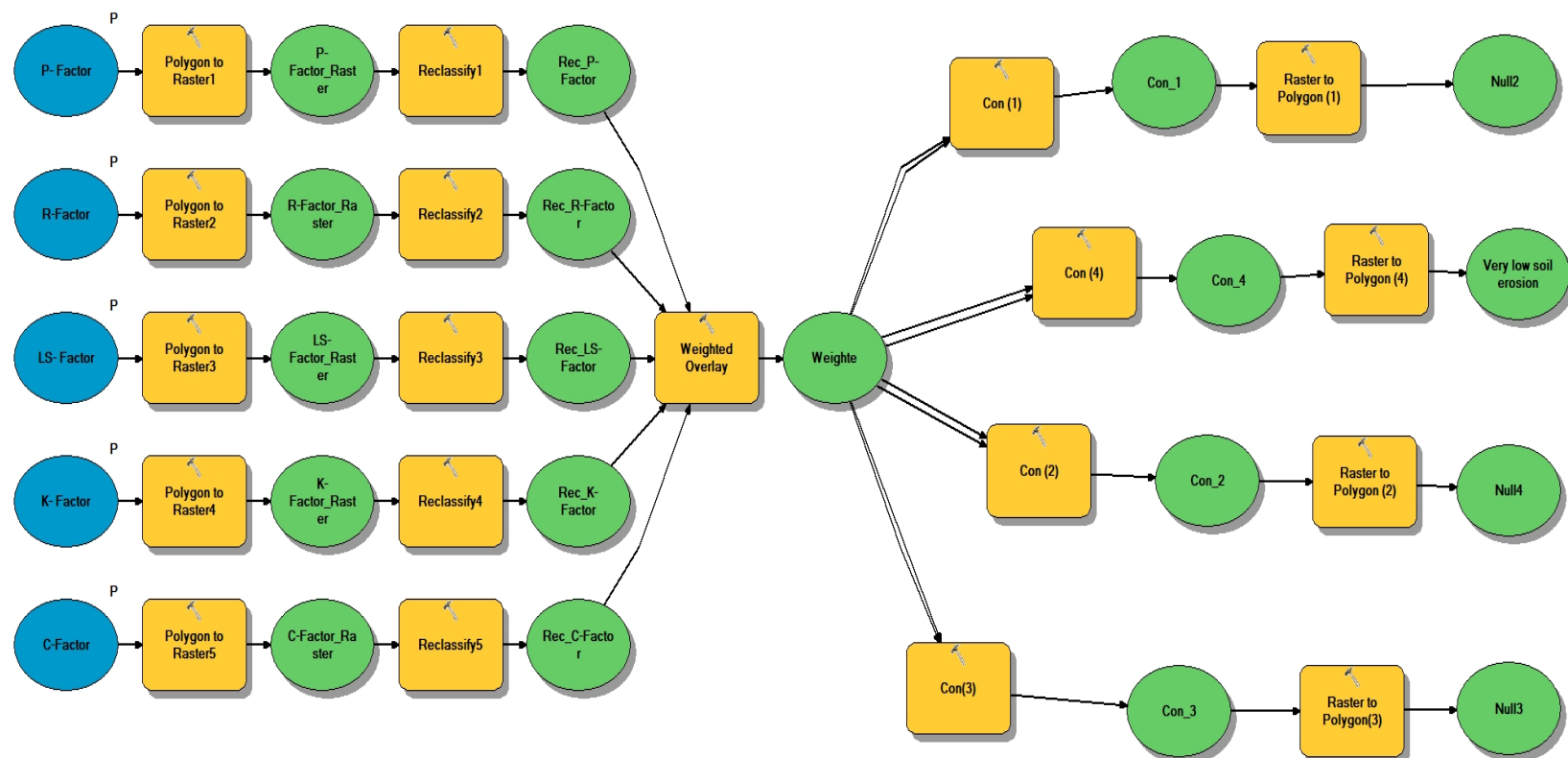


Figure 4. A flowchart of the proposed spatial-based model (SSLM) design steps according to the USLE model.

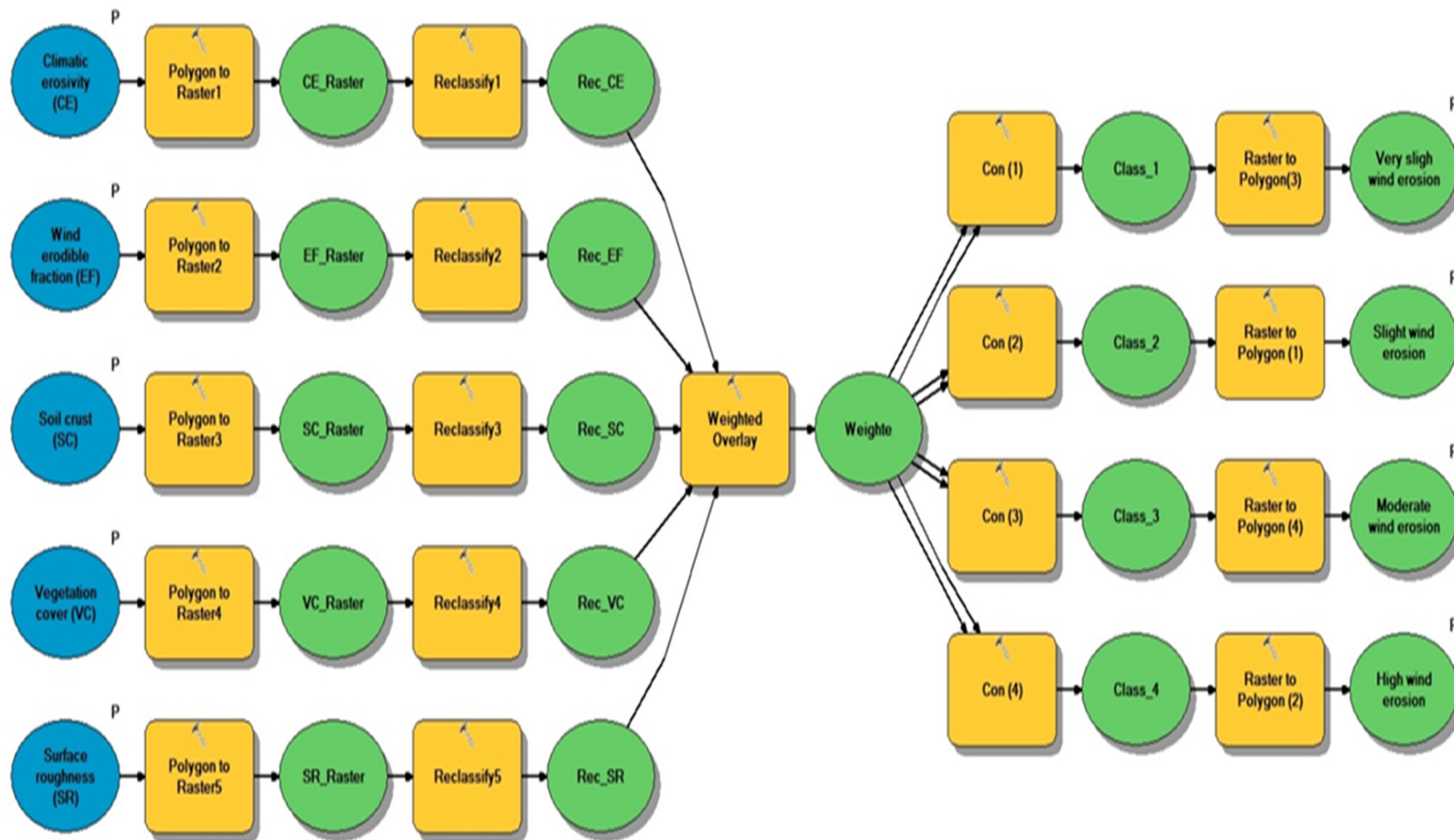


Figure 5. A flowchart of the proposed spatial-based model (SSLM) design steps according to the ILSWE model.

3. Results and Discussion

3.1. Study Area Characteristics

The terrain data of the study area showed that land is flat to almost flat in the physiographic configuration, with a slope ranging from 0.1% to 2.2% and a slope length ranging from 60 to 981 m. This physiography was interrupted by residual relief in the form of isolated hills (Inselberg) and waterbodies. There were five soil texture grades: clay, loam, silty clay loam, sandy clay loam, and sandy loam. As organic residue was lacking, the organic matter (OM) content of these soils ranged from 1.02 to 20.4 g kg⁻¹. The annual average precipitation rate (rainfall rate) was very low (1 mm yr⁻¹). Agricultural lands, crops and pastures, rocky outcrops, and bare lands were the land use/land cover in the investigated region, as defined by satellite image classification and the NDVI [63]. Ridge tillage, fall plow, mulch tillage, and no-till systems were the tillage systems employed in the study area. Agricultural management conservation support and land practices included contour farming, strip cropping, cross slopes, and up-and-down slopes. Table 10 shows the support practices employing the land use/land cover and slope-classified images, which include different types of agricultural management practices based on altering flow patterns, gradients, or the direction of surface runoff with specific support and land practice effects. With minor restrictions on the soil quality grade, approximately 80% to 85% of the total study area was identified as suitable soil for agricultural use [64].

Table 10. Land properties of the investigated area.

P. No.	Slope (%)	Slope Length (m)	Texture	OM (g kg ⁻¹)	Crop Management	Tillage Method	Support Practice	Rainfall (mm yr ⁻¹)
1	0.4	75	SL	3.60	Bare lands	Ridge tillage	Contour farming	1.01
2	0.5	80	L	3.45	Crops	Fall plow	Contour farming	1.00
3	0.3	92	SCL	8.40	Agriculture lands	Fall plow	Contour farming	1.00
4	0.4	60	SCL	8.70	Bare lands	Ridge tillage	Contour farming	1.00
5	0.5	122	SL	3.40	Bare lands	Ridge tillage	Contour farming	1.00
6	0.5	160	C	12.6	Agriculture lands	Fall plow	Contour farming	1.00
7	2.2	88	C	20.4	Agriculture lands	Fall plow	Strip cropping	1.00
8	0.9	245	C	19.8	Crops	Fall plow	Contour farming	1.00
9	1.1	360	SL	2.40	Bare lands	No-till	Cross slope	1.00
10	0.1	340	SiL	1.03	Bare lands	Ridge tillage	Contour farming	0.99
11	0.1	258	L	6.47	Agriculture lands	Fall plow	Contour farming	1.00
12	0.1	378	SL	6.50	Crops and Pasture	Mulch tillage	Contour farming	1.00
13	0.2	364	C	12.3	Agriculture lands	Fall plow	Contour farming	1.00
14	0.1	465	L	3.21	Crops	Fall plow	Contour farming	1.00
15	0.1	410	C	6.42	Agriculture lands	Fall plow	Contour farming	1.00
16	0.1	136	SCL	5.30	Crops	Fall plow	Contour farming	1.00
17	0.1	187	C	6.10	Crops and Pasture	Mulch tillage	Up and down slope	1.00
18	2.1	289	SCL	10.4	Agriculture lands	Fall plow	Strip cropping	1.00
19	0.1	246	L	2.60	Bare lands	Ridge tillage	Contour farming	0.99
20	0.1	358	SCL	4.20	Agriculture lands	Fall plow	Contour farming	0.99
21	0.1	560	SL	3.80	Crops	Fall plow	Contour farming	1.00
22	0.1	810	L	3.10	Agriculture lands	Fall plow	Contour farming	1.00
23	0.1	981	SL	2.91	Bare lands	No-till	Contour farming	1.00
24	0.1	274	SL	2.54	Crops and Pasture	Mulch tillage	Contour farming	1.00
25	0.1	176	SL	1.02	Bare lands	No-till	Contour farming	0.99

P = profile; OM = organic matter; SL = sandy loam; L = loam; SCL = sandy clay loam; C = clay; SiL = silty clay loam.

3.2. Determination and Spatial Distribution of the USLE Model Factors

Table 11 shows the descriptive statistical data on the rates of the various factors used in the USLE calculation. In addition, the spatial distribution maps of those factors across the study area are illustrated in Figures 4–9. The variability of USLE factors was classified into three categories based on the coefficient of variation (CV): low variation ($CV < 15\%$) for the R-Factor; moderate variation ($15 \leq CV \leq 35\%$) for the K-Factor, C1-Factor, and P-Factor; and high variation ($CV > 35\%$) for the C2-Factor and LS-Factor [65]. The USLE model factors' mean values were ranked as follows: $R > C > P > K > LS$ (Table 11).

Table 11. Descriptive data on the rates of USLE factors, the USLE model, and SSLM.

Parameter	Minimum	Maximum	Mean	Standard Deviation	Coefficient of Variation (%)	Standard Error
K-Factor	0.29	0.85	0.48	0.16	32.46	0.03
LS-Factor	0.09	0.37	0.14	0.07	47.08	0.01
C1-Factor	0.42	1.00	0.70	0.22	31.53	0.04
C2-Factor	0.25	1.00	0.73	0.32	43.95	0.06
P-Factor	0.37	1.00	0.52	0.12	22.80	0.02
R-Factor	79.361	79.365	79.363	0.00	0.00	0.00
USLE	0.26	3.51	1.30	0.83	64.30	0.17
SSLM	0.26	3.09	1.33	0.71	53.38	0.14

USLE = universal soil loss equation; SSLM: spatial soil loss model.

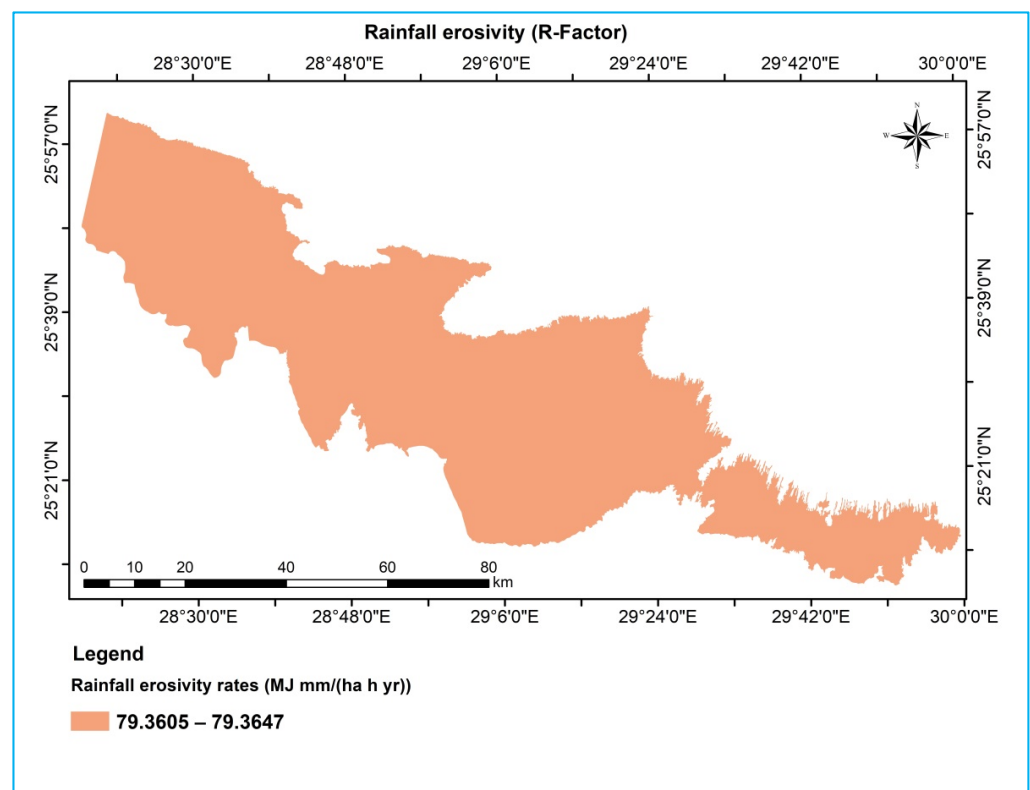


Figure 6. Spatial distribution map of rainfall erosivity factor (R-Factor).

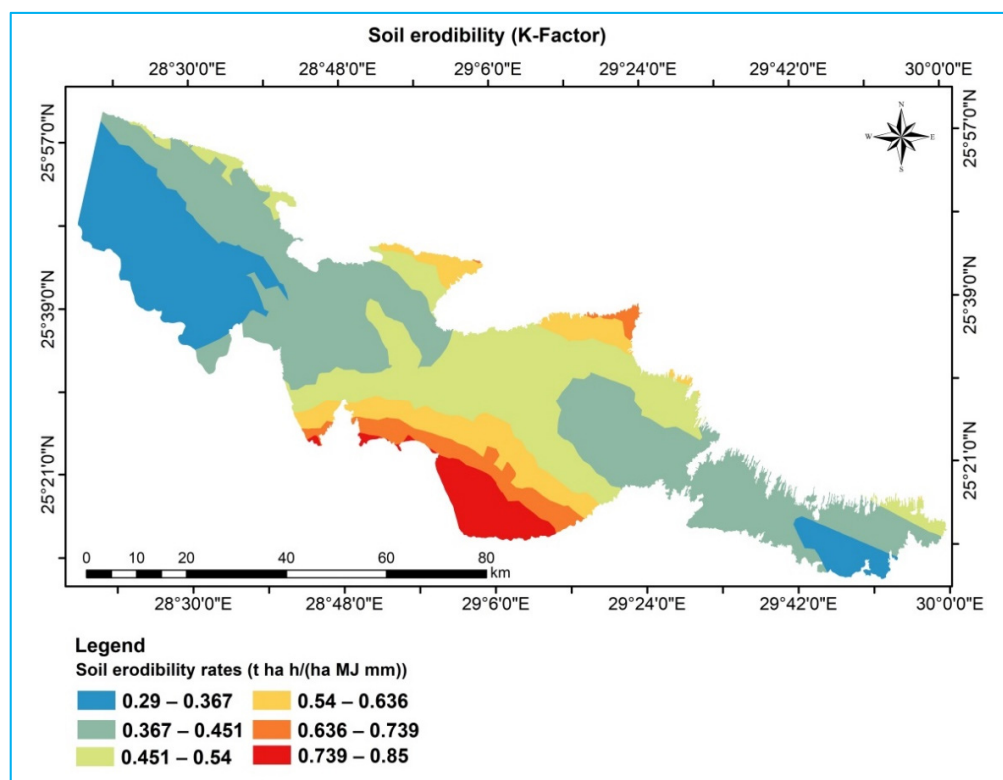


Figure 7. Spatial distribution map of soil erodibility factor (K-Factor).

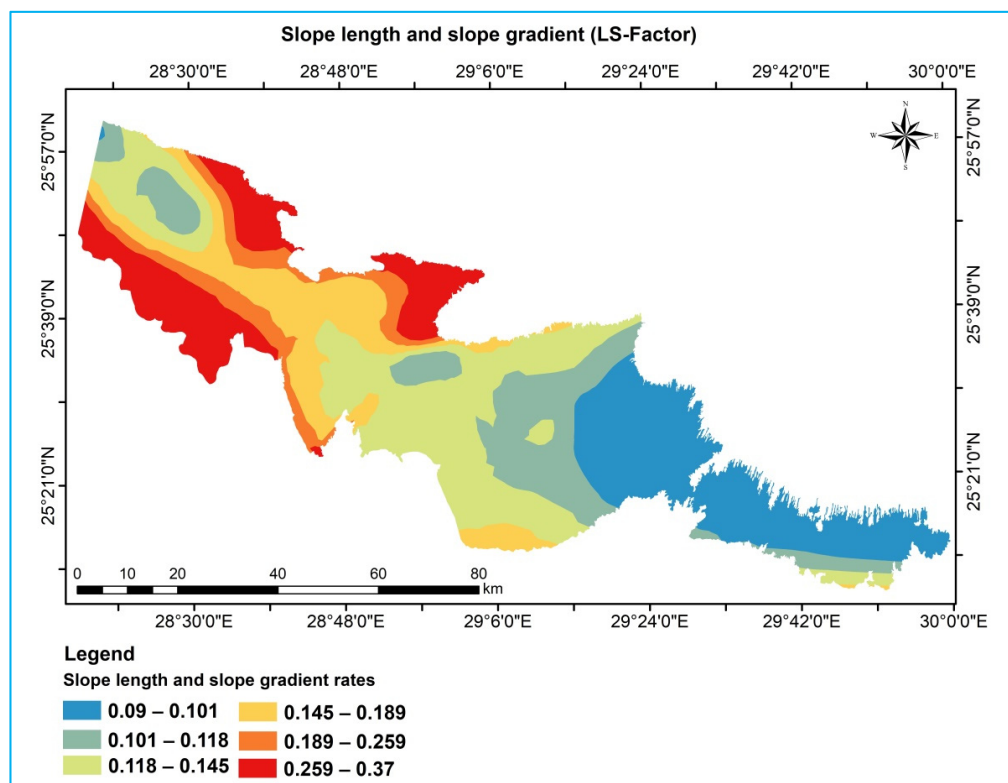


Figure 8. Spatial distribution map of slope length and slope gradient factors (LS-Factor).

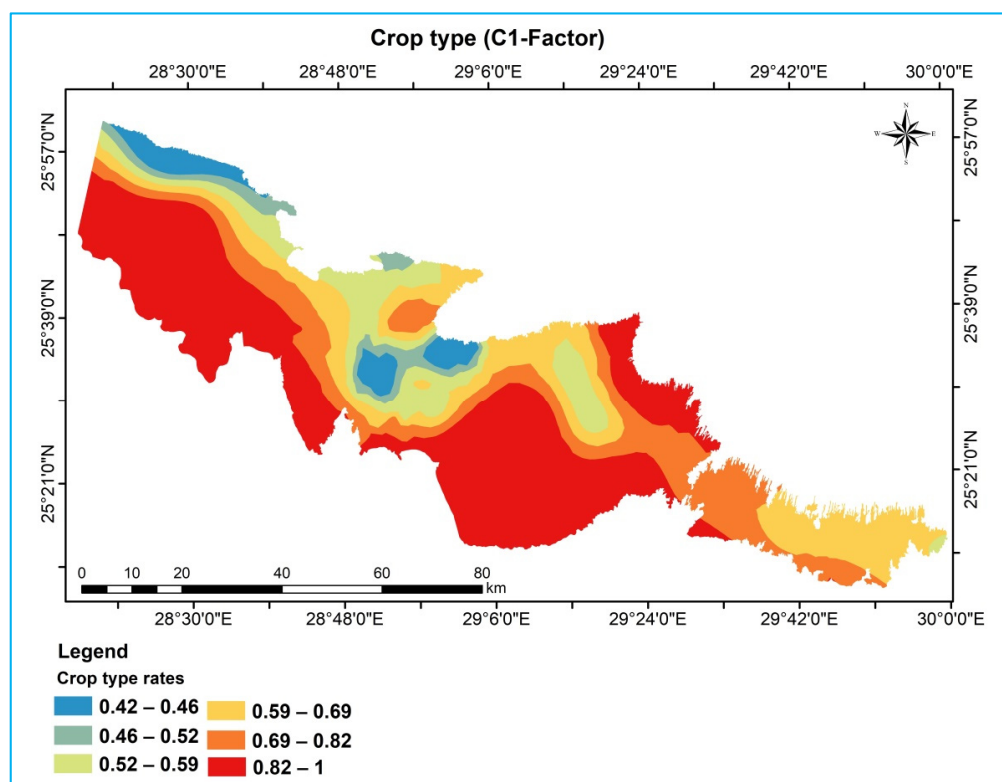


Figure 9. Spatial distribution map of the crop-type factor (C1-Factor).

3.2.1. Rainfall Erosivity Factor (*R*-Factor)

The rainfall erosivity factor (*R*-Factor) refers to the aggressiveness of runoff sediment deposits due to motion action. The motion action aggressiveness of the runoff sediment deposits in the study area was measured by the rainfall erosivity factor. According to the spatial distribution determined using the kriging interpolation method and the estimated *R*-Factor values, the *R*-Factor rates in the study area ranged from 79.361 to 79.365 MJ mm ha^{−1} h^{−1} yr^{−1} with an average of 79.363 MJ mm ha^{−1} h^{−1} yr^{−1}. These results are in agreement with those found by Xu et al. [50] in a study that adapted the RUSLE and GIS to model soil erosion risk in the mountain karst watershed in Guizhou Province, China. The *R*-Factor spatial distribution map revealed no changes across the study area, indicating that the region received the same low amount of rainfall as shown in Figure 6. Furthermore, as shown in Table 11, the *R*-Factor values were very close to each other, with the standard deviation, coefficient of variation (%), and standard error all equaling zero. According to these findings, the intensity of the rainfall erosivity factor in the soil loss rate is very low. Soil loss is closely associated with rainfall, notably due to the detachment power and runoff of raindrops striking the soil surface [66]. As a result, soil loss was very low in the study area, which is typical of an arid desert [40,43].

3.2.2. Soil Erodibility Factor (*K*-Factor)

The *K*-Factor for the soil profiles was calculated using the average particle size, soil structure stability, soil permeability, and organic matter values. As shown in Figure 7 and Table 11, the soil erodibility values ranged between 0.29 and 0.85 t ha h ha^{−1} MJ^{−1} mm^{−1} with a mean of 0.48 t ha h ha^{−1} MJ^{−1} mm^{−1}. Moreover, with a CV of 32.46%, the *K*-Factor showed moderate variability across the study area (Table 11). According to the *K*-Factor spatial variation map, the *K*-Factor values gradually decreased from the depression's upper outer borders to its floor (Figure 7). The spatial variation indicated that the inherent erodibility of the soil at the upper oasis depression was high (red color grades), while that of the soil at the lower sites was low (blue color grades). This is because the soils on the

depression floor are agriculturally active, which correlates with soil structure stability and increased organic matter, resulting in less soil susceptibility to detachment and increased infiltration. These findings are compatible with those reported by Panagos et al. [52], where they studied soil erodibility in Europe based on land use/cover to assess soil erosion. Furthermore, the upper outer zones and uplands soils (yellow and red color grades) of Dakhla Oasis have the highest K-Factor rates because they are barren lands with extremely low organic matter and coarse-textured soils. According to these findings, it was obvious that the soil texture is the most important factor influencing the K-Factor rate in the investigation area.

3.2.3. Slope Length and Slope Gradient Factor (*LS*-Factor)

The effects of local topography on runoff per unit, cutting rates, and accumulation are explained by the *LS*-Factor. The topographic factor rates (slope length and slope gradient) in the study area varied from 0.09 in flat areas to 0.37 on steep slopes lands, with an average of 0.14 (Figure 7). The distribution patterns of the *SL*-Factor were characterized by high variations, with a CV of 47.08% as presented in Table 11 and Figure 8. The *LS*-Factor spatial distribution map revealed that the highest *LS*-Factor values were found in the outer zones of the northern and southern parts (red, orange, yellow colors) of the study area's western half, where the land is steep. Low values were observed in the depression's eastern half and across its floor, where the land is flat in the plain areas (Figure 8). Moreover, the high *LS*-Factor values decreased gradually from the outer (steep lands) to the inner (flat lands), which corresponds with the slope gradients in the study area. This means that in a three-dimensional complex terrain with flow convergence and divergence, the upslope contributing area, and not the slope length, controls soil loss [67]. Gelagay and Minale [67] reported that in the narrower steeper slope in the upper part of the watershed, very severe soil loss was observed at a rate that exceeded the tolerable soil loss limit. They attributed this to the steepness of the slope, the dominance of soil types that are inherently less resistant to the eroding power of rainfall, and the lack of supportive practice [67].

3.2.4. Cover Management Factor (*C*-Factor)

According to soil conservation practices, the *C*-Factor describes the effect of land cover and management practices on different types of crops and tillage methods. Based on the NDVI index extracted from the Landsat-8 satellite image of the study area, as well as field measurements, the *C*-Factor is effective in relating to biophysical properties when exported to thematic maps (crop type and tillage method). The crop-type factor (*C1*-Factor) for different types of crops ranged from 0.42 to 1 with a mean of 0.70, while the tillage system factor (*C2*-Factor) for no-till and fall plow lands was between 0.25 and 1, with an average of 0.73, as shown in Table 11. Furthermore, with a CV of 31.53%, the *C1*-Factor showed moderate variability, while the *C2*-Factor revealed high variability with a CV of 43.95% across the study area. These results were similar to those found by Kouli et al. [55] in a study that was conducted to predict soil erosion using the revised universal soil loss equation (RUSLE) in a GIS framework in Chania, northwestern Crete, Greece. They reported that the vegetation cover factor together with slope steepness and length factors is most sensitive to soil loss [55].

The spatial variability of the *C*-Factor based on the *C1*-Factor and according to the *C2*-Factor is shown in Figures 9 and 10, respectively. The high rates of *C1*-Factor were found in the study area's southern zones with some in the northern ones (red color grades), where these zones are classified as barren lands. The low values (blue color grades), on the other hand, were discovered in plain areas in the middle of the study area, which are characterized by the presence of agricultural activities (Figure 9). Concerning the spatial variability of the *C2*-Factor, it was in contrast to the *C1*-Factor, where the high values were found in agricultural areas due to the application of tillage methods, particularly fall plowing, while low values were found in barren areas, which were characterized by no-till methods (Figure 10).

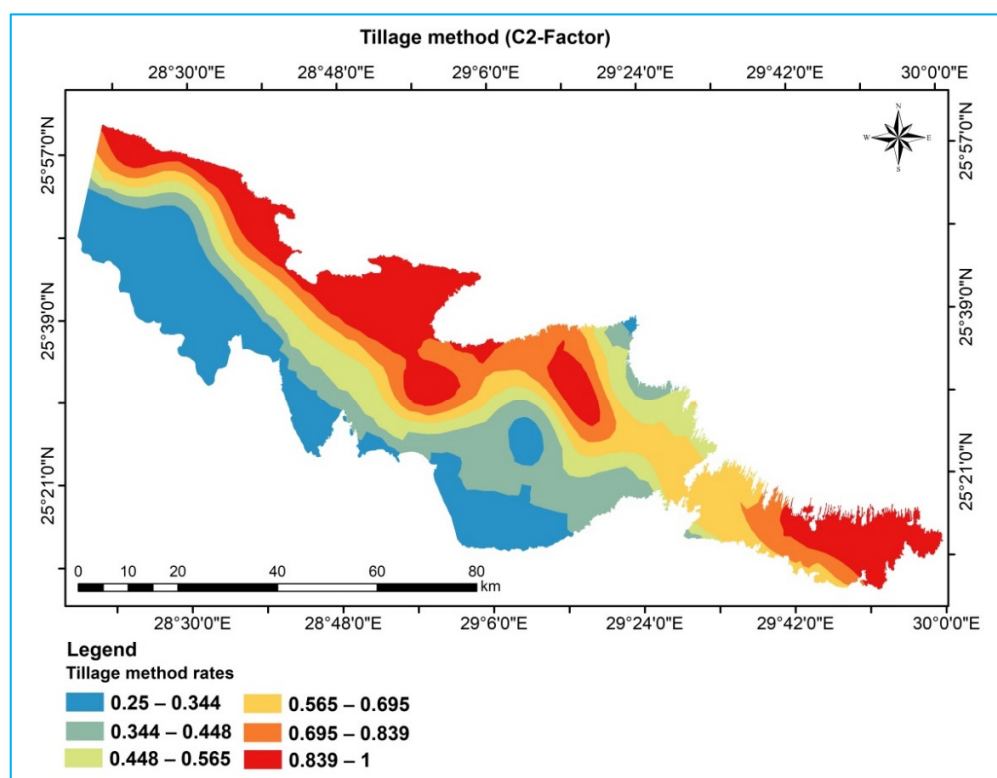


Figure 10. Spatial distribution map of the tillage method factor (C2-Factor).

3.2.5. Conservation Practice (*P*-Factor)

According to the land use/land cover and slope maps, the *P*-Factor represents up-and-down slope tillage through surface runoff altering flow patterns, gradients, or directions with a specific support land practices' effect. The *P*-Factor values of the investigated area ranged from 0.37 to 1.00 with mean of 0.52 (Table 11). Furthermore, with a CV of 22.80%, the *P*-Factor was characterized by moderate variability throughout the study area. The selection of appropriate conservation measures such as support practice, contour farming, strip cropping, cross slope, and up-and-down slope, can help to reduce the soil erosion caused by soil loss. The obtained results are consistent with those found by Dabral et al. [14] in a study that used USLE, GIS, and remote sensing to assess soil erosion in a hilly catchment in northeastern India. According to this study, the highest and lowest conservation factor (*P*) values were found to be 1 and 0.28, respectively. Figure 11 shows a map of the spatial distribution of *P*-Factor values.

3.3. Soil Erosion Assessment

3.3.1. Water Erosion

1. Based on the USLE model

The annual average soil loss due to rill erosion was calculated by overlaying the values of the five factors: *R*, *K*, *LS*, *C*, and *P*. Based on the soil characteristics, land use, and topography map of the investigated area, these factors were employed in the USLE model and SSM. According to USLE model, the soil loss rate varied widely spatially, as shown in Figure 12 and Table 11, with values ranging from 0.26 to 3.51 t ha^{−1} yr^{−1}, and an average of 1.30 t ha^{−1} yr^{−1}. Furthermore, the soil loss spatial variability was high with a CV of 64.30%. Based on classification standards, the average potential soil erosion rate (1.30 t ha^{−1} yr^{−1}) indicated that the Dakhla Oasis as a whole is very slightly eroded. Therefore, the study area was combined into one soil erosion class, which was very low (<6.7 t ha^{−1} yr^{−1}). Accordingly, the very low soil erosion class is the dominant class in this study area, as shown in Table 12. The prevalence of a very low class was related to

land flatness and scarcity of rainfall. According to the spatial variability map (Figure 12), the soil loss rate was high in steeply sloping areas and places with little vegetation cover. Furthermore, the soil loss rates differed among agricultural lands, bare lands, crops and pasture lands, and rocky outcrops lands. As a result, the Dakhla Oasis is qualified as a promising area for sustainable agriculture if appropriate management is applied.

2. Based on the SSLM

The SSLM-based assessment of soil erosion produced results that are very similar to those obtained from the USLE model. According to SSLM, the soil loss rate widely varied spatially, as shown in Figure 13 and Table 11, with values ranging from 0.26 to 3.09 t ha⁻¹ yr⁻¹, and an average of 1.30 t ha⁻¹ yr⁻¹. Similar to the USLE model, the soil loss spatial variability was high with a CV of 53.38%. Furthermore, the study area was combined into a single soil erosion class as very low, as the USLE model presented. Figure 13 shows the spatial distribution of the soil loss rates according the SSLM. If the soil loss spatial distribution map based on the USLE model and the soil loss spatial distribution map according to the SSLM are compared, they are nearly congruent. This demonstrated that the proposed spatial-based model (SSLM) is fit and accurate for predicting, quantifying, and mapping soil loss under this study.

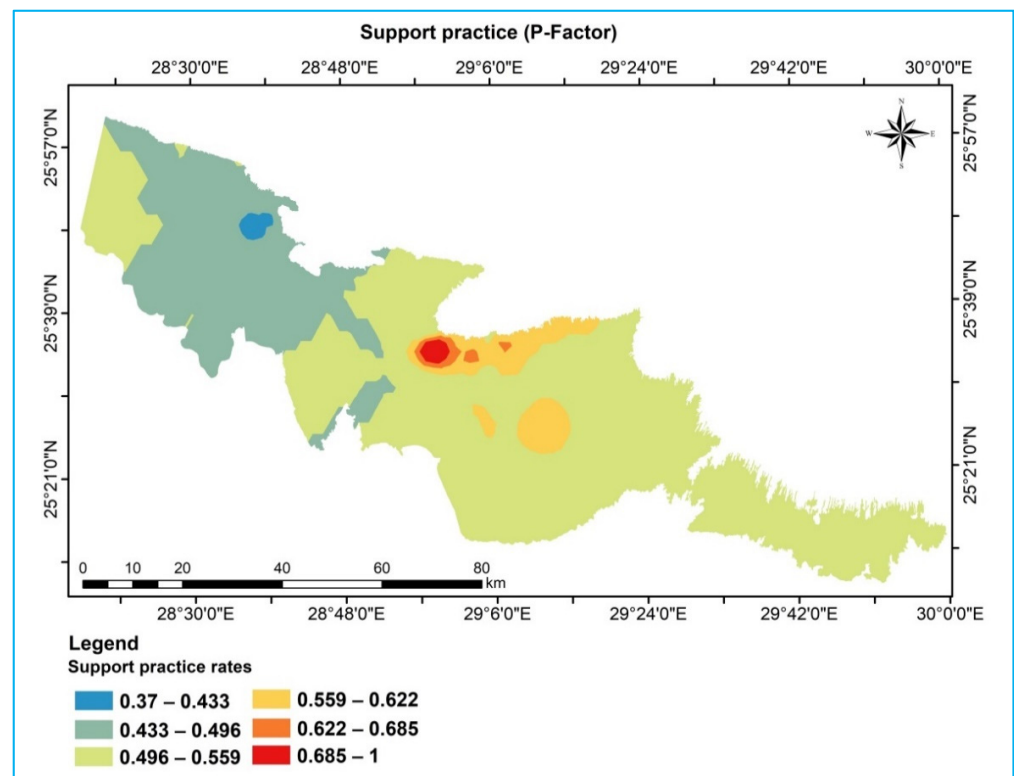


Figure 11. Spatial distribution map of conservation practice factor (*P*-Factor).

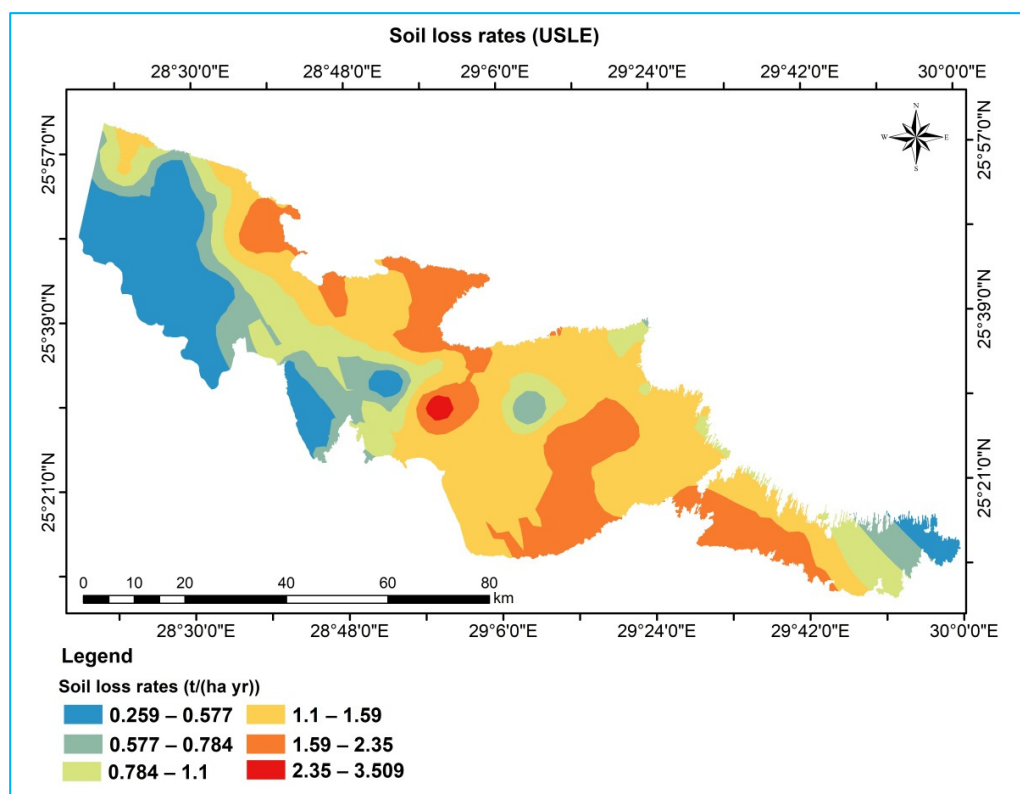


Figure 12. Spatial distribution map of soil loss rates according to the USLE model.

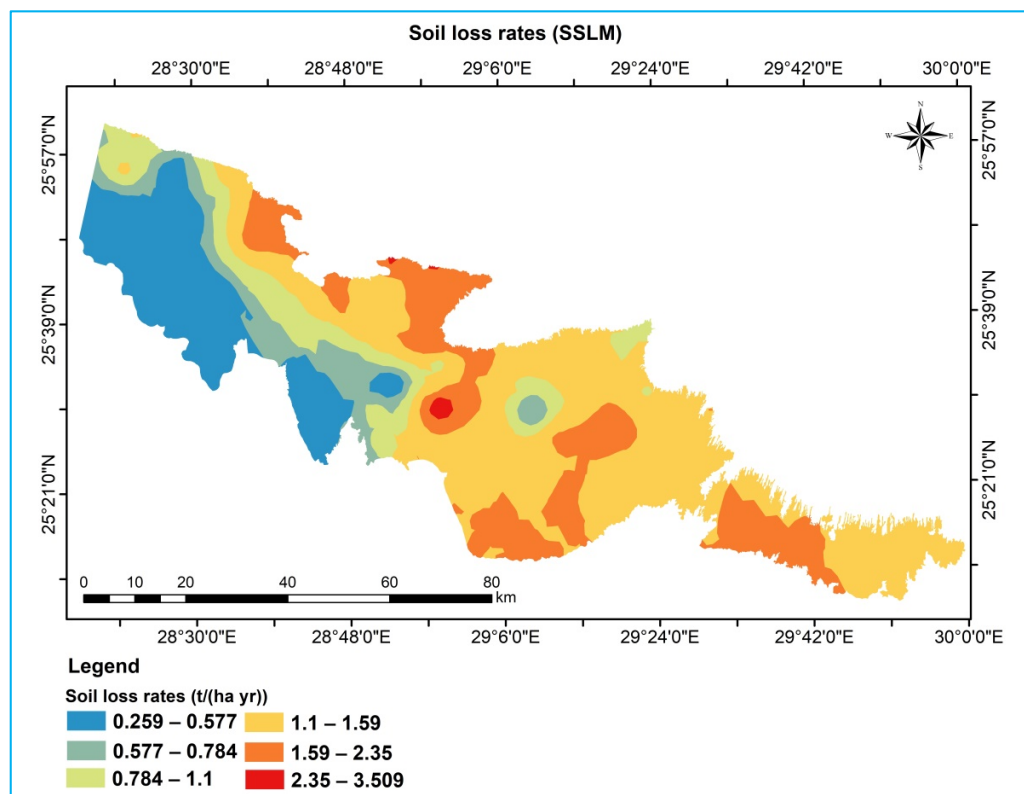


Figure 13. Spatial distribution map of soil loss rates according to the proposed model (SSLM).

Table 12. Soil erosion rates and classes according to the USLE model and the proposed model (SSLM).

P. No.	USLE	SSLM	S.E.C.	P. No.	USLE	SSLM	S.E.C.	P. No.	USLE	SSLM	S.E.C.
1	0.64	0.72	Very low	10	1.30	1.27	Very low	19	1.02	1.07	Very low
2	2.34	2.12	Very low	11	1.75	1.58	Very low	20	1.28	1.42	Very low
3	1.71	1.97	Very low	12	0.32	0.29	Very low	21	0.76	0.96	Very low
4	1.00	1.09	Very low	13	1.28	1.19	Very low	22	1.91	1.85	Very low
5	0.36	0.26	Very low	14	3.51	3.09	Very low	23	0.40	0.55	Very low
6	1.05	1.10	Very low	15	1.28	1.25	Very low	24	0.32	0.83	Very low
7	2.38	2.67	Very low	16	0.88	0.95	Very low	25	0.26	0.68	Very low
8	1.18	1.22	Very low	17	0.88	1.17	Very low				
9	1.61	1.44	Very low	18	2.93	2.54	Very low				

P = profile; S.E.C. = soil erosion class.

3.3.2. Wind Erosion

1. Based on the ILSWE model

The spatial distribution of wind erosion hazards according to the ILSWE model is presented in Figure 14. Based on the ILSWE model values, the study area was classified into four classes. The four classes of wind erosion severity were very slight, slight, moderate, and high, representing 1.0%, 25.2%, 41.5%, and 32.3% of the total study area, respectively. According to the spatial distribution map (Figure 14), the east and west parts of the oasis, which are characterized by bare land and a scarcity of vegetation, are at high risk of wind erosion (red color). The moderate soil erosion class (orange color) was the dominant class in this study area, as shown in Figure 14. Furthermore, the very slight and slight classes were observed in areas with dense vegetation cover, especially in palm trees and orchard cultivation areas. Accordingly, the Dakhla Oasis requires appropriate management and conservation practice against wind erosion for sustainable agriculture. According to Fenta et al. [32], who developed the index of land susceptibility to wind erosion (ILSWE) and used it to estimate and assess soil erosion severity and risks in the East Africa region, they reported that around 25% of the study area is experiencing risks of soil erosion by wind. Moreover, they stated that wind erosion risks are mainly attributable to poor vegetation cover (VC-Factor) and, hence, high surface roughness (SR-Factor). Table 13 shows the values and classes of wind erosion hazards based on the ILSWE for each soil profile. The wind erosion indexes ranged from 0.04 (very low) to 28.12 (high) with a mean of 11.88 (Table 13).

2. Based on the SSLM

The SSLM-based assessment of soil erosion produced results that are very similar to those obtained from the ILSWE model. Based on the SSLM, wind erosion indexes widely varied spatially, as shown in Figure 15 and Table 13, with values ranging from 0.43 to 27.87, and an average of 12.31 (Table 13). Similar to the ILSWE model, the study area was classified into four classes. The four classes of wind erosion severity were very slight, slight, moderate, and high, representing 0.9%, 25.4%, 43.9%, and 29.9% of the total study area, respectively. If the soil loss spatial distribution map based on the ILSWE model and the soil loss spatial distribution map according to the SSLM are compared, they are nearly congruent. This demonstrated that the proposed spatial-based model (SSLM) is suitable and accurate for predicting, quantifying, and mapping wind erosion under this study.

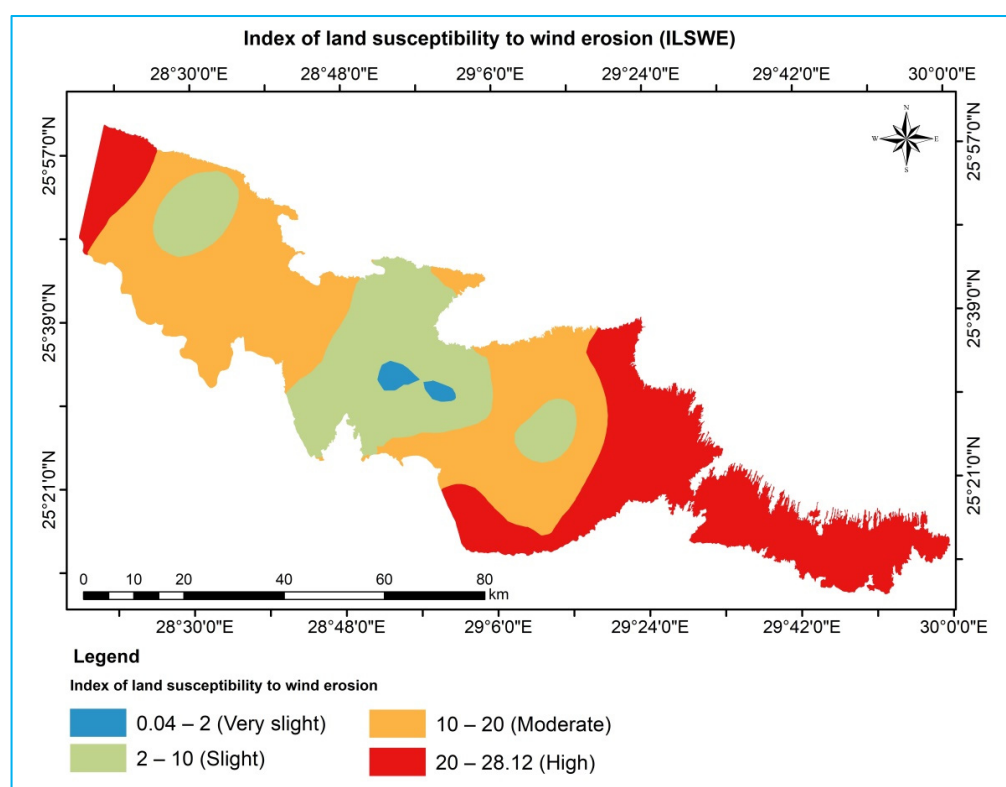


Figure 14. Spatial distribution map of wind erosion indexes and classes according to the ILSWE model.

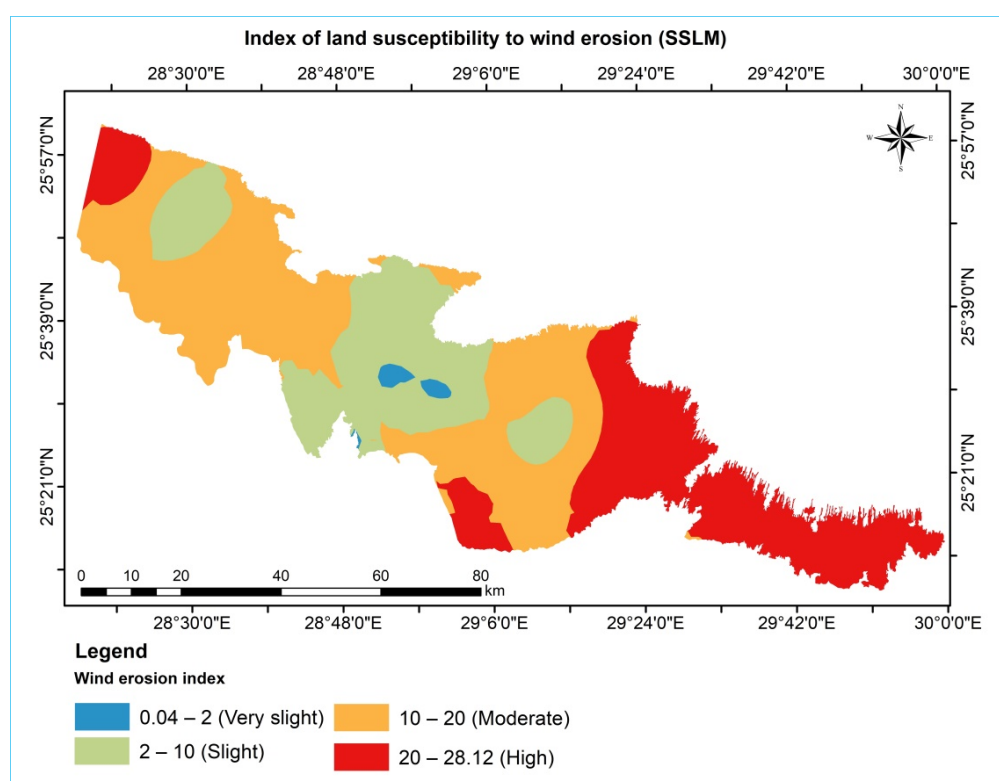


Figure 15. Spatial distribution map of wind erosion indexes and classes according to the SSLM.

Table 13. Wind erosion indexes and classes according to the ILSWE model and the proposed model (SSLM).

P. No.	ILSWE	SSLM	S.E.C.	P. No.	ILSWE	SSLM	S.E.C.	P. No.	ILSWE	SSLM	S.E.C.
1	28.12	27.00	High	10	21.75	23.68	High	19	12.75	10.71	Moderate
2	16.98	17.26	Moderate	11	1.36	1.53	Very slight	20	28.08	27.87	High
3	20.89	19.00	High	12	0.41	0.47	Very slight	21	9.07	9.06	Slight
4	26.88	26.83	High	13	0.04	0.43	Very slight	22	12.46	12.27	Moderate
5	13.81	12.41	Moderate	14	2.56	3.87	Slight	23	21.52	24.44	High
6	9.08	11.19	Slight	15	5.79	5.58	Slight	24	13.77	11.58	Moderate
7	15.32	15.17	Moderate	16	0.79	1.20	Very slight	25	0.04	0.72	Very slight
8	17.83	19.75	Moderate	17	10.33	14.13	Moderate				
9	1.61	1.78	Very slight	18	5.76	9.74	Slight				

P = profile; S.E.C. = soil erosion class.

Overall, many studies have concluded that different land use/land cover have varied impacts on soil erosion [68–70]. There are four land use/land cover types in the study area, and in the following order of total area: barren land (82.7%) > agricultural land (13.4%) > sand dunes (3.1%) > built-up land (0.7%), considering the Dakhla Oasis in 2018 [56]. The soil types in the study area with high clay concentrations in the top layers may increase the water runoff and, consequently, the erodibility [70,71]. Due to the very low annual precipitation in the study area, the effective soil erosion factors are the K-Factor, C-Factor, and P-Factor, which are associated with soil characteristics and management practices [70]. Furthermore, very low soil erosion risk intensity was most prominent, indicating that there is currently no erosion hazard due to water erosion, while wind erosion ranged from very slight to high across the study area. Although anthropogenic activities may be important locally, the main causes of soil erosion spatial variability in the study area might be associated with natural factors such as soil types and land cover. According to the outputs of the different models, the study area is slightly eroded due to water erosion and moderately eroded by wind.

3.4. Model Validation

The geometric mean algorithm of the five factors was used to calculate soil erosion, and statistical calibration was performed using the average linear regression (ALR) method. The ALR value, which represented the R^2 , was 0.94 and 0.97 for the USLE and ILSWE models with the SSLM, respectively (Figures 16 and 17). These values indicate a very high correlation between the estimated erosion rates based on both the USLE and ILSWE models and the proposed model (SSLM). The outputs of the soil erosion according to the USLE model and the SSLM, as well as the ILSWE model and the SSLM, were close to each other (Tables 12 and 13) and had a strong positive correlation ($r = 0.97$ and 0.98 , respectively). These results revealed a strong relationship between the USLE model and the SSLM and between the ILSWE model and the SSLM, which indicated that the proposed spatial-based model (SSLM) is valid to quantify the soil loss rate. Furthermore, the high congruence between the outputs and maps of the spatial distribution of the USLE and the ILSWE models with the SSLM indicated that the proposed spatial-based model (SSLM) has a high accuracy for predicting and calculating soil erosion rates. Policy planners can utilize the predicted soil erosion maps, because they provide a useful guide for future sustainable landscape development and natural resource management.

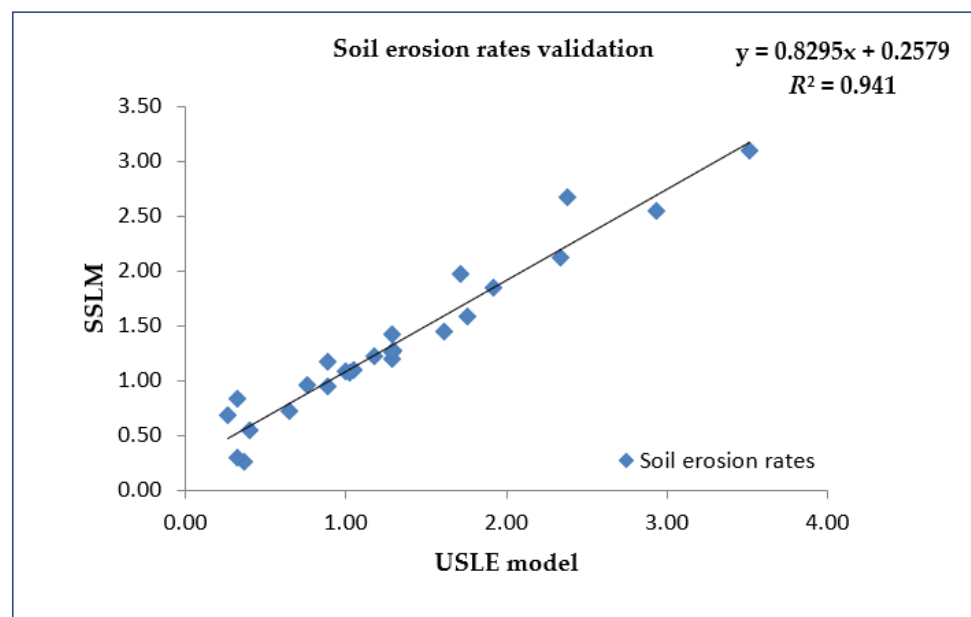


Figure 16. Linear relationship between the USLE model and the proposed model (SSLM).

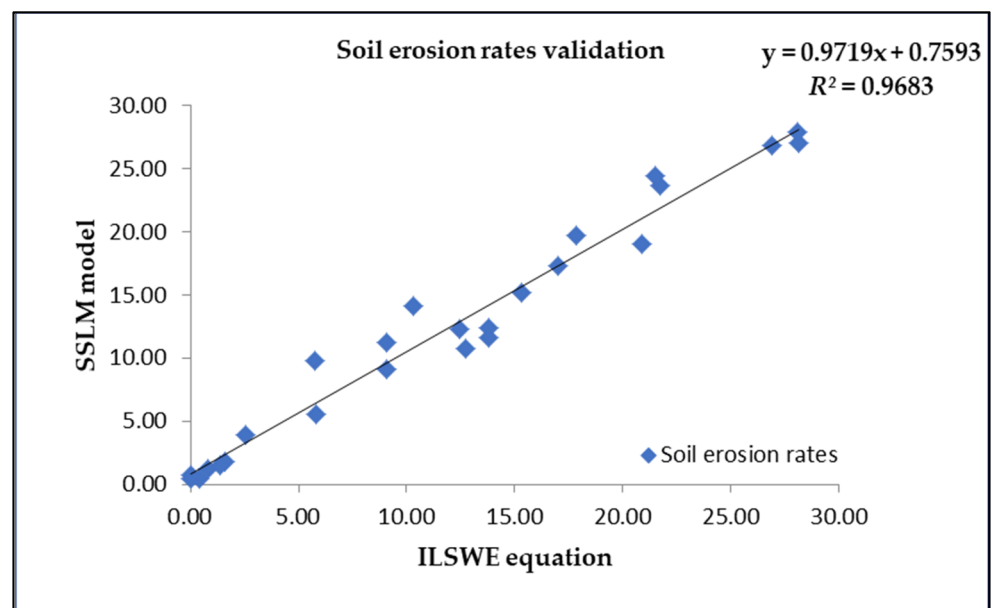


Figure 17. Linear relationship between the ILSWE model and the proposed model (SSLM).

4. Conclusions

The present study is an attempt to adopt a spatial-based model to compute and map potential soil erosion. It proposed a spatial-based model to quantify the soil loss rate and to identify and map the spatial distribution of soil erosion in the Dakhla Oasis, Egypt. The proposed spatial-based model (SSLM) was designed by integrating GIS analyst environment with the universal soil loss equation (USLE) and Index of Land Susceptibility to Wind Erosion (ILSWE) models. The annual average of soil loss due to rill erosion was calculated using the USLE model and SSLM by overlaying the five factors' values (R , K , LS , C , and P). The outputs of the soil loss according to the USLE model and the SSLM were close to each other. Soil loss values based on the USLE model and the SSLM varied from 0.26 to $3.51 \text{ t ha}^{-1} \text{ yr}^{-1}$ with an average of $1.30 \text{ t ha}^{-1} \text{ yr}^{-1}$ and from 0.26 to $3.09 \text{ t ha}^{-1} \text{ yr}^{-1}$ with a mean of $1.33 \text{ t ha}^{-1} \text{ yr}^{-1}$, respectively. Therefore, and according to the assessment of

both the USLE and the SSLM, one soil erosion class, the very low class ($<6.7 \text{ t ha}^{-1} \text{ yr}^{-1}$), was reported to be the prevalent erosion class in the study area. These findings indicate that the Dakhla Oasis is slightly eroded and more tolerable against soil erosion factors under current management conditions. Therefore, based on a vulnerability assessment of water erosion in the study area, the very low soil erosion class was the most prevalent in the study area due to the land flatness and rainfall scarcity.

Furthermore, the study area was classified into four classes of wind erosion severity—very slight, slight, moderate, and high—representing 1.0%, 25.2%, 41.5%, and 32.3% of the total study area, respectively, based on the ILSWE model, and 0.9%, 25.4%, 43.9% and 29.9%, respectively, according to SSLM. The moderate wind erosion class was the dominant class in this study area. Moreover, very slightly and slightly classes were observed in areas with dense vegetation cover, especially in palm trees and orchard cultivation areas. Accordingly, the Dakhla Oasis requires appropriate management and conservation practices against wind erosion for sustainable agriculture. According to the outputs of the different models, the study area is slightly eroded due to water erosion and moderately eroded by wind. Consequently, the Dakhla Oasis is qualified as a promising area for sustainable agriculture when appropriate management is applied. Crop types, soil types, drainage patterns, and land barrenness are the most important factors of soil erosion in the study area, though anthropogenic activities may play a role locally.

Comparing the findings obtained from both the USLE and ILSWE models to those of the SSLM, there were strong positive correlations ($r = 0.97$ and 0.98 , respectively), as well as strong relationships based on the average linear regression ($R^2 = 0.94$ and 0.97 , respectively). Furthermore, the high congruence between the outputs and maps of the spatial distribution of the USLE and ILSWE models and those of the SSLM indicated that the proposed spatial-based model (SSLM) has a high accuracy for predicting and calculating soil erosion rates. This study also pointed out that designing soil erosion spatial models using available data sources and the integration of the USLE and ILSWE models with GIS techniques is a viable option for calculating soil loss rates and classes. Finally, the proposed soil erosion spatial model is suitable for calculating and assessing soil loss rates under this study and is valid for use in other studies under similar arid regions.

Author Contributions: Conceptualization, S.A.H.S., S.H.A.A.-A. and M.E.F.; methodology, S.A.H.S., S.H.A.A.-A. and M.E.F.; software, S.A.H.S. and M.E.F.; validation, S.A.H.S., S.H.A.A.-A., R.J.-B., F.J.G.-N. and M.E.F.; formal analysis, S.A.H.S. and M.E.F.; investigation, S.A.H.S., S.H.A.A.-A. and M.E.F.; resources, S.A.H.S., S.H.A.A.-A., R.J.-B., F.J.G.-N. and M.E.F.; data curation, S.A.H.S., S.H.A.A.-A., R.J.-B., F.J.G.-N. and M.E.F.; writing—original draft preparation, S.A.H.S., S.H.A.A.-A., M.E.F. and R.J.-B.; writing—review and editing, S.A.H.S., S.H.A.A.-A., R.J.-B., F.J.G.-N. and M.E.F.; visualization, S.A.H.S., S.H.A.A.-A., F.J.G.-N. and M.E.F.; supervision, S.H.A.A.-A., R.J.-B. and F.J.G.-N. All authors have read and agreed to the published version of the manuscript.

Funding: This research received no external funding.

Institutional Review Board Statement: Not applicable.

Informed Consent Statement: Not applicable.

Data Availability Statement: Not applicable.

Acknowledgments: The authors very much appreciate the significant contributions made by the journal's editors and reviewers to manage and review this article.

Conflicts of Interest: The authors declare no conflict of interest.

References

1. Rahman, M.R.; Shi, Z.H.; Chongfa, C. Soil erosion hazard evaluation—An integrated use of remote sensing, GIS and statistical approaches with biophysical parameters towards management strategies. *Ecol. Modell.* **2009**, *220*, 1724–1734. [\[CrossRef\]](#)
2. Panagos, P.; Borrelli, P.; Meusburger, K.; Yu, B.; Klik, A.; Lim, K.J.; Yang, J.E.; Ni, J.; Miao, C.; Chattopadhyay, N.; et al. Global rainfall erosivity assessment based on high-temporal resolution rainfall records. *Sci. Rep.* **2017**, *7*, 1–12. [\[CrossRef\]](#) [\[PubMed\]](#)
3. Lal, R. Soil degradation by erosion. *Land Degrad. Dev.* **2001**, *12*, 519–539. [\[CrossRef\]](#)
4. Lal, R. Soil erosion and the global carbon budget. *Environ. Int.* **2003**, *29*, 437–450. [\[CrossRef\]](#)
5. FAO; ITPS. *Status of the World's Soil Resources (SWSR)—Main Report*, 1st ed.; Luco, M., Victor, C., Kazuyuki, Y., Pavel, K., Seyed, K.A.P., de Lourdes, M.M., Dan, P., Neil, M., Eds.; Food and Agriculture Organization of the United Nations and Intergovernmental Technical Panel on Soils: Rome, Italy, 2015; p. 607.
6. Cerdà, A.; Flanagan, D.C.; Le Bissonnais, Y.; Boardman, J. Soil erosion and agriculture. *Soil Tillage Res.* **2009**, *106*, 107–108. [\[CrossRef\]](#)
7. Edwards, W.M.; Owens, L.B. Large storm effects on total soil erosion. *J. Soil Water Conserv.* **1991**, *46*, 75–78.
8. Ananda, J.; Herath, G. Soil erosion in developing countries: A socio-economic appraisal. *J. Environ. Manag.* **2003**, *68*, 343–353. [\[CrossRef\]](#)
9. Merritt, W.S.; Letcher, R.A.; Jakeman, A.J. A review of erosion and sediment transport models. *Environ. Model Softw.* **2003**, *18*, 761–799. [\[CrossRef\]](#)
10. Rizeei, H.M.; Saharkhiz, M.A.; Pradhan, B.; Ahmad, N. Soil erosion prediction based on land cover dynamics at the Semenyih watershed in Malaysia using LTM and USLE models. *Geocarto Int.* **2016**, *31*, 1158–1177. [\[CrossRef\]](#)
11. Karydas, C.G.; Panagos, P.; Gitas, I.Z. A classification of water erosion models according to their geospatial characteristics. *Int. J. Digit. Earth* **2014**, *7*, 229–250. [\[CrossRef\]](#)
12. Labrière, N.; Locatelli, B.; Laumonier, Y.; Freycon, V.; Bernoux, M. Soil erosion in the humid tropics: A systematic quantitative review. *Agric. Ecosyst. Environ.* **2015**, *203*, 127–139. [\[CrossRef\]](#)
13. Wischmeier, W.H.; Smith, D.D. *Predicting Rainfall Erosion Losses—A Guide to Conservation Planning*; Agriculture Handbook No. 537; USDA-Science and Education Administration: Hyattsville, MD, USA, 1978; p. 67.
14. Dabral, P.P.; Baithuri, N.; Pandey, A. Soil erosion assessment in a hilly catchment of north eastern India using USLE, GIS and remote sensing. *Water Resour. Manag.* **2008**, *22*, 1783–1798. [\[CrossRef\]](#)
15. Karamage, F.; Zhang, C.; Kayiranga, A.; Shao, H.; Fang, X.; Ndayisaba, F.; Nahayo, L.; Mupenzi, C.; Tian, G. USLE-based assessment of soil erosion by water in the Nyabarongo River catchment, Rwanda. *Int. J. Environ. Res. Public Health* **2016**, *13*, 835. [\[CrossRef\]](#) [\[PubMed\]](#)
16. Pham, T.G.; Degener, J.; Kappas, M. Integrated universal soil loss equation (USLE) and Geographical Information System (GIS) for soil erosion estimation in a sap basin: Central Vietnam. *Int. Soil Water Conserv. Res.* **2018**, *6*, 99–110. [\[CrossRef\]](#)
17. Melalih, A.; Mazour, M. Using RUSLE and GIS for the soil loss assessment in arid regions: The case of the Ain Sefra catchment in the Ksour Mountains, Algeria. *J. Water Land Dev.* **2021**, *48*, 205–214. [\[CrossRef\]](#)
18. Jemai, S.; Kallel, A.; Agoubi, B.; Abid, H. Soil erosion estimation in arid area by USLE model applying GIS and RS: Case of Oued El Hamma catchment, south-eastern Tunisia. *J. Indian Soc. Remote. Sens.* **2021**, *29*, 1293–1305. [\[CrossRef\]](#)
19. Othman, A.A.; Obaid, A.K.; Al-Manmi, D.A.M.A.; Al-Maamar, A.F.; Hasan, S.E.; Liesenberg, V.; Shihab, A.T.; Al-Saady, Y.I. New insight on soil loss estimation in the northwestern region of the Zagros fold and thrust belt. *ISPRS Int. J. Geo-Inf.* **2021**, *10*, 59. [\[CrossRef\]](#)
20. Renard, K.G.; Foster, G.R.; Weesies, G.A.; McCool, D.K.; Yoder, D.C. *Predicting Soil Erosion by Water: A Guide to Conservation Planning with the Revised Universal Soil Loss Equation (RUSLE)*; United States Department of Agriculture: Washington, DC, USA, 1997; p. 384.
21. Gessesse, B.; Bewket, W.; Bräuning, A. Model-based characterization and monitoring of runoff and soil erosion in response to land use/land cover changes in the Modjo watershed, Ethiopia. *Land Degrad. Dev.* **2015**, *26*, 711–724. [\[CrossRef\]](#)
22. Sepuru, T.K.; Dube, T. An appraisal on the progress of remote sensing applications in soil erosion mapping and monitoring. *Remote Sens. Appl. Soc. Environ.* **2018**, *9*, 1–9. [\[CrossRef\]](#)
23. Vrieling, A.; Sterk, G.; de Jong, S.M. Satellite-based estimation of rainfall erosivity for Africa. *J. Hydrol.* **2010**, *395*, 235–241. [\[CrossRef\]](#)
24. Rahman, M.R.; Shi, Z.H.; Chongfa, C.; Dun, Z. Assessing soil erosion hazard -a raster based GIS approach with spatial principal component analysis (SPCA). *Earth Sci. Inform.* **2015**, *8*, 853–865. [\[CrossRef\]](#)
25. Pradhan, B.; Chaudhari, A.; Adinarayana, J.; Buchroithner, M.F. Soil erosion assessment and its correlation with landslide events using remote sensing data and GIS: A case study at Penang Island, Malaysia. *Environ. Monit. Assess.* **2012**, *184*, 715–727. [\[CrossRef\]](#) [\[PubMed\]](#)
26. Zeng, Z.Y.; Cao, J.Z.; Gu, Z.J.; Zhang, Z.L.; Zheng, W.; Cao, Y.Q.; Peng, H.Y. Dynamic monitoring of plant cover and soil erosion using remote sensing, mathematical modeling, computer simulation and GIS techniques. *Am. J. Plant Sci.* **2013**, *4*, 1466–1493. [\[CrossRef\]](#)
27. Seutloali, K.E.; Dube, T.; Mutanga, O. Assessing and mapping the severity of soil erosion using the 30-m Landsat multispectral satellite data in the former South African homelands of Transkei. *Phys. Chem. Earth* **2017**, *100*, 296–304. [\[CrossRef\]](#)

28. Tralli, D.M.; Blom, R.G.; Zlotnicki, V.; Donnellan, A.; Evans, D.L. Satellite remote sensing of earthquake, volcano, flood, landslide and coastal inundation hazards. *ISPRS J. Photogramm. Remote Sens.* **2005**, *59*, 185–198. [\[CrossRef\]](#)
29. Brits, A.; Burke, M.; Li, T. Improved modelling for urban sustainability assessment and strategic planning: Local government planner and modeller perspectives on the key challenges. *Aust. Plan.* **2014**, *51*, 76–86. [\[CrossRef\]](#)
30. Pradhan, B.; Abokharima, M.H.; Jebur, M.N.; Tehrany, M.S. Land subsidence susceptibility mapping at Kinta Valley (Malaysia) using the evidential belief function model in GIS. *Nat. Hazards* **2014**, *73*, 1019–1042. [\[CrossRef\]](#)
31. Danumah, J.H.; Odai, S.N.; Saley, B.M.; Szarzynski, J.; Thiel, M.; Kwaku, A.; Kouame, F.K.; Akpa, L.Y. Flood risk assessment and mapping in Abidjan district using multi-criteria analysis (AHP) model and geoinformation techniques, (cote d’ivoire). *Geoenviron. Disasters* **2016**, *3*, 10. [\[CrossRef\]](#)
32. Fenta, A.A.; Tsunekawa, A.; Haregeweyn, N.; Poesen, J.; Tsubo, M.; Borrelli, P.; Panagos, P.; Vanmaercke, M.; Broeckx, J.; Yasuda, H.; et al. Land susceptibility to water and wind erosion risks in the East Africa region. *Sci. Total Environ.* **2020**, *703*, 135016. [\[CrossRef\]](#)
33. Khan, S.D.; Fathy, M.S.; Abdelazeem, M. Remote sensing and geophysical investigations of Moghra Lake in the Qattara Depression, Western Desert, Egypt. *Geomorphology* **2014**, *207*, 10–22. [\[CrossRef\]](#)
34. Abdel Meguid, M. Key features of the Egypt’s water and agricultural resources. In *Conventional Water Resources and Agriculture in Egypt*, 1st ed.; Negm, A.M., Ed.; Springer: Berlin/Heidelberg, Germany, 2017; pp. 39–99. [\[CrossRef\]](#)
35. AbdelRahman, M.A.E.; Natarajan, A.; Hegde, R.; Prakash, S.S. Assessment of land degradation using comprehensive geostatistical approach and remote sensing data in GIS-model builder. *Egypt. J. Remote Sens. Space Sci.* **2019**, *22*, 323–334. [\[CrossRef\]](#)
36. Mohamed, E.S.; Schüttb, B.; Belal, A. Assessment of environmental hazards in the north western coast -Egypt using RS and GIS, Egypt. *Egypt. J. Remote Sens. Space Sci.* **2013**, *16*, 219–229. [\[CrossRef\]](#)
37. Abuzaid, A.S.; Fadl, M.E. Land evaluation of eastern Suez Canal, Egypt using remote sensing and GIS. *Egypt. J. Soil Sci.* **2016**, *56*, 537–548. [\[CrossRef\]](#)
38. Abuzaid, A.S.; Abdellatif, A.D.; Fadl, M.E. Modelling soil quality in Dakahlia Governorate, Egypt using GIS Techniques. *Egypt. J. Remote. Sens. Space Sci.* **2021**, *24*, 255–264. [\[CrossRef\]](#)
39. Abuzaid, A.S.; Fadl, M.E. Mapping potential risks of long-term wastewater irrigation in alluvial soils, Egypt. *Arab. J. Geosci.* **2018**, *11*, 433. [\[CrossRef\]](#)
40. Zaghloul, E. A Geology of Dakhla Oasis, Western Desert, Egypt. In *Sustainable Water Solutions in the Western Desert, Egypt: Dakhla Oasis*, 1st ed.; Iwasaki, E., Negm, A.M., Elbeih, S.F., Eds.; Part of the Earth and Environmental Sciences Library book series (EESL); Springer: Cham, Switzerland, 2021; pp. 29–44. [\[CrossRef\]](#)
41. Soil Survey Staff. *Keys to Soil Taxonomy*, 12th ed.; USDA-Natural Resources Conservation Service: Washington, DC, USA, 2014; p. 360.
42. National Oceanic and Atmospheric Administration (NOAA). Dakhla Climate Normals Appendix I: Meteorological Data. Available online: <https://www.noaa.gov/> (accessed on 17 January 2019).
43. Selmy, S.A.H. Studies on Some Shale-Derived Soils in the New Valley, Egypt. Master’s Thesis, Assiut University, Assiut, Egypt, 2005.
44. Selmy, S.; Abd El-Aziz, S.; Gameh, M.; Abdelsalam, A. Characterization and mapping spatial variability of Entisols derived from shale in Dakhla Oasis, Egypt. *Arab. J. Geosci.* **2020**, *13*, 592. [\[CrossRef\]](#)
45. ITT. *ITT Corporation*; Westchester Avenue: White Plains, NY, USA, 2017.
46. ESRI. *ArcMap Version 10.2.2. User Manual*; ESRI: Redlands, CA, USA, 2014.
47. Soil Science Division Staff. *Soil Survey Manual*; Ditzler, C., Scheffe, K., Monger, H.C., Eds.; Government Printing Office: Washington, DC, USA, 2017; p. 587.
48. Soil Survey Staff. *Soil Survey Field and Laboratory Methods Manual—Soil Survey Investigations. Report No. 51*, 2 nd ed.; Burt, R., Soil Survey Staff, Eds.; USDA-Natural Resources Conservation Service: Washington, DC, USA, 2014; p. 457.
49. Robert, P.; Stone, P.; Don, H. *Universal Soil Loss Equation (USLE)*; Ministry of Agriculture, Food and Rural Affairs: Ontario, ON, Canada, 2012. Available online: <http://www.omafra.gov.on.ca/english/engineer/facts/12-051.htm> (accessed on 20 January 2019).
50. Xu, Y.Q.; Shao, X.M.; Kong, X.B.; Peng, J.; Cai, Y.L. Adapting the RUSLE and GIS to model soil erosion risk in a mountains karst watershed, Guizhou Province, China. *Environ. Monit. Assess.* **2008**, *141*, 275–286. [\[CrossRef\]](#)
51. Choudhury, M.K.; Nayak, T. Estimation of soil erosion in Sagar Lake catchment of Central India. In *Proceedings of the International Conference on Water and Environment, Bhopal, India, 15–18 December 2003*; pp. 387–392.
52. Panagos, P.; Meusburger, K.; Ballabio, C.; Borrelli, P.; Alewell, C. Soil erodibility in Europe: A high-resolution dataset based on LUCAS. *Sci. Total Environ.* **2014**, *479–480*, 189–200. [\[CrossRef\]](#)
53. Efthimiou, N. The importance of soil data availability on erosion modeling. *Catena* **2018**, *165*, 551–566. [\[CrossRef\]](#)
54. Wischmeier, W.H.; Johnson, C.B.; Cross, B.V. A soil erodibility nomograph for farmland and construction sites. *J. Soil Water Cons.* **1971**, *26*, 189–193.
55. Kouli, M.; Soupios, P.; Vallianatos, F. Soil erosion prediction using the revised universal soil loss equation (RUSLE) in a GIS frame-work, Chania, Northwestern Crete, Greece. *Environ. Geol.* **2009**, *57*, 483–497. [\[CrossRef\]](#)
56. Funk, R.; Reuter, H.I. Wind erosion. In *Soil Erosion in Europe*; Boardman, J., Poesen, J., Eds.; Wiley: Chichester, UK, 2006; pp. 563–582. [\[CrossRef\]](#)

57. Skidmore, E.L. Wind erosion climatic erosivity. *Clim. Chang.* **1986**, *9*, 195–208. [[CrossRef](#)]
58. FAO. *A Provisional Methodology for Soil Degradation Assessment*; Food and Agriculture Organization: Rome, Italy, 1979.
59. Fryrear, D.W.; Krammes, C.A.; Williamson, D.L.; Zobeck, T.M. Computing the wind erodible fraction of soils. *J. Soil Water Conserv.* **1994**, *49*, 183–188.
60. Zhang, K.L.; Li, S.; Peng, W.; Yu, B. Erodibility of agricultural soils on the Loess Plateau of China. *Soil Till. Res.* **2004**, *76*, 157–165. [[CrossRef](#)]
61. Fryrear, D.W.; Saleh, A.; Bilbro, J.D.; Schomberg, H.M.; Stout, J.E.; Zobeck, T.M.; Revised Wind Erosion Equation (RWEQ). Wind Erosion and Water Conservation Research Unit, USDA-ARS, Southern Plains Area Cropping Systems Research Laboratory. Technical Bulletin, 1998, No. 1. p. 185. Available online: <https://www.csrl.ars.usda.gov/wewc/rweq/rweq.pdf> (accessed on 22 June 2019).
62. Jain, P.; Ramsankaran, R. GIS-based modelling of soil erosion processes using the modified-MMF (MMMF) model in a large watershed having vast agro-climatological differences. *Earth Surf. Process. Landf.* **2018**, *43*, 2064–2076. [[CrossRef](#)]
63. Shalaby, A.; Khedr, H.S. Remote Sensing and GIS for Land Use/Land Cover Change Detection in Dakhla Oasis. In *Sustainable Water Solutions in the Western Desert, Egypt: Dakhla Oasis*, 1st ed.; Iwasaki, E., Negm, A.M., Elbeih, S.F., Eds.; Part of the Earth and Environmental Sciences Library book series (EESL); Springer: Cham, Switzerland, 2021; pp. 145–159. [[CrossRef](#)]
64. Selmy, S.A.H.; Abd Al-Aziz, S.H.; Jiménez-Ballesta, R.; Jesús García-Navarro, F.; Fadl, M.E. Soil Quality Assessment Using Multivariate Approaches: A Case Study of the Dakhla Oasis Arid Lands. *Land* **2021**, *10*, 1074. [[CrossRef](#)]
65. Wilding, L.P. Spatial variability: Its documentation, accommodation, and implication to soil surveys. In *Soil Spatial Variability*; Nielsen, D.R., Bouma, J., Eds.; Pudoc: Wageningen, The Netherlands, 1985; pp. 166–194.
66. Wang, Y.; Yang, F.; Qi, S.; Cheng, J. Estimating the Effect of Rain Splash on Soil Particle Transport by Using a Modified Model: Study on Short Hillslopes in Northern China. *Water* **2020**, *12*, 2318. [[CrossRef](#)]
67. Gelagay, H.S.; Minale, A.S. Soil loss estimation using GIS and Remote sensing techniques: A case of Koga watershed, Northwestern Ethiopia. *Int. Soil Water Conserv. Res.* **2016**, *4*, 126–136. [[CrossRef](#)]
68. Fu, B.J.; Wang, Y.F.; Lu, Y.H.; He, C.S.; Chen, L.D.; Song, C.J. The effects of land-use combinations on soil erosion: A case study in the Loess Plateau of China. *PPG Earth Environ.* **2009**, *33*, 793–804. [[CrossRef](#)]
69. Wang, B.; Zheng, F.L.; Römkens, M.J.M. Comparison of soil erodibility factors in USLE, RUSLE2, EPIC and Dg models based on a Chinese soil erodibility database. *Acta Agric. Scand. B Soil Plant Sci.* **2012**, *63*, 69–79. [[CrossRef](#)]
70. Falcão, K.S.; Panachuki, E.; Monteiro, F.N.; Menezes, R.S.; Rodrigues, D.B.B.; Sone, J.S.; Oliveira, P.T.S. Surface runoff and soil erosion in a natural regeneration area of the Brazilian Cerrado. *Int. Soil Water Conserv. Res.* **2020**, *8*, 124–130. [[CrossRef](#)]
71. Parveen, R.; Kumar, U. Integrated Approach of Universal Soil Loss Equation (USLE) and Geographical Information System (GIS) for Soil Loss Risk Assessment in Upper South Koel Basin, Jharkhand. *J. Geogr. Inf. Syst.* **2012**, *4*, 588–596. [[CrossRef](#)]